Physical Nature of Interactions in Zn[II] Complexes with 2,2′-Bipyridyl: Quantum Theory of Atoms in Molecules (QTAIM), Interacting Quantum Atoms (IQA), Noncovalent Interactions (NCI), and Extended Transition State Coupled with Natural Orbitals for Chemical Valence (ETS-NOCV) Comparative Studies

Ignacy Cukrowski[a]*, Jurgens H. de Lange[a] and Mariusz Mitoraj[b]*

[a] Department of Chemistry, Faculty of Natural and Agricultural Sciences, University of

Pretoria, Lynnwood Road, Pretoria 0002, South Africa

[b] K. Gumiński Department of Theoretical Chemistry, Faculty of Chemistry, Jagiellonian

University, R. Ingardena 3, 30-060 Cracow, Poland

1

Abstract:

In the present account factors determining the stability of ZnL, ZnL_2, ZnL_3 complexes (L = bpy, 2,2′-bipyridyl) were characterized based on various techniques: the Quantum Theory of Atoms in Molecules (QTAIM), energy decomposition schemes based on Interacting Quantum Atoms (IQA) and Extended Transition State coupled with Natural Orbitals for Chemical Valence (ETS-NOCV). Finally, the Non-covalent Interactions (NCI) index was also applied. All methods consistently indicated that the strength of the coordination bonds, Zn–O, Zn–N, decreases from ZnL to ZnL_3. Importantly, it has been identified that the strength of secondary intramolecular heteropolar hydrogen bonding interactions, CH•••O, CH•••N, increases when going from ZnL to ZnL_3. A similar trend appeared to be valid for the π-bonding as well as electrostatic stabilization. In addition to the above leading bonding contributions, all techniques suggested the existence of very subtle, but non-negligible additional stabilization from the CH•••HC electronic exchange channel; these interactions are the weakest among all considered here. From IQA it was found that the local diatomic interaction energy, $E_{\text{int}}^{\text{H,H}}$, amounts at HF to –2.5, –2.7 and –2.9 kcal mol^{-1} for ZnL, ZnL_2 and ZnL_3, respectively (–2.1 kcal mol^{-1} for ZnL at MP2). NOCV-based deformation density channels showed that formation of CH--HC contacts in Zn-complexes causes significant polarization of σ(C–H) bonds, which accordingly leads to charge accumulation in the CH•••HC bay region. Charge depletion from σ(C–H) bonds were also reflected in the calculated spin-spin ^{1}J(C–H) coupling constants, which decrease from 177.06 Hz (ZnL) to 173.87 Hz (ZnL_3). This last result supports our findings of an increase in the local electronic CH•••HC stabilization from ZnL to ZnL_3 found from QTAIM, IQA, and ETS-NOCV. Finally, this work unites for the first time the results from four methods that are widely used for description of chemical bonding.

1. Introduction

The ligand 2,2′-bipyridyl (L or bpy) is an important representative of α-diimines and it has excellent ability to form complexes, hence its chemistry with tens of metal ions has been investigated experimentally for years resulting in hundreds of the formation constants reported.[1] Moreover, metal complexes of bpy have been investigated for the purpose of solar energy devices, energy storages, or possible nonlinear optical materials.[2–4] Knowledge of the conformational structure of α-diimine ligands and information about the rotational energy barrier are important and useful for a better understanding of the complex formation process and trends in stability of complexes. Hence not surprisingly, these ligands have also been extensively studied computationally[5–18] and for over 40 years it is known that the most stable conformer of 2,2′-bipyridyl has two N-atoms *trans* to each other (s-*trans* conformer).[9–15] Lower stability of the conformer with nitrogens *cis* to each other (s-*cis* conformer) was attributed mainly to the steric hindrance of the 3,3′-hydrogen atoms and destabilizing nitrogen lone pair-lone pair interactions[11–17] in 2,2′-bipyridyl. To act as a chelate, this ligand must, however, attain the s-*cis* conformation resulting in the 3,3′-hydrogen atoms being in the close contact, CH--HC (Figure. 1).
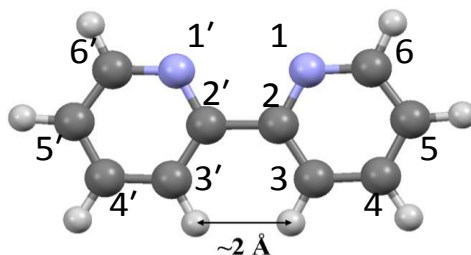
Figure 1. Higher energy conformer of the free ligand bpy, as found in metal complexes, with N-atoms *cis* to each other (s-*cis* conformer) showing steric clash between 3,3′-hydrogen atoms.

It is well-known fact that many, if not majority, of metal complexes with this ligand in crystals show nearly-planar structure of 2,2′-bipyridyl with geometric H-clashes present. These H-

clashes are assumed to be also present in a solution and were often used to explain trends in experimental formation constants.[19–27] For instance, the unusual trend in the formation constants of Cu^{II} was attributed to steric repulsion between the 3,3′-hydrogens already fifty years ago.[19] More recently, the observed difference of about 1.4 log units for a set of metal ions with 1,10-phenanthroline (phen) and 2,2′-bipyridyl (the latter ligand forms weaker complexes) was attributed to highly strained ligand in the s-*cis* conformer (as it is required for coordination to metal ions) because of the steric hindrance between the hydrogen atoms.[24] In very recent report, where H-clashes in phenanthrene and 2,2′-bipyridyl were investigated, Hancock and Nikolayenko[28] concluded that these contacts should be seen as unfavorable H--H nonbonded interactions of the H atoms, in principle, in all known cases where they are in a steric clash because '*the concept of energetically unfavorable nonbonded H--H interactions at short H--H separations has been very productive in explaining organic stereochemistry, and so the idea that such interactions are energetically favorable would, if correct, overturn much chemical thinking built up over many decades*'. It is important to note that Bader and co-workers interpreted close contacts CH--HC in some molecules as the bonding interactions, either from the calculated[29–37] or experimental[29,38–40] electron density distributions, using the quantum theory of atoms in molecules (QTAIM).[41] The formation of H–H bonding interactions in simple molecules (like biphenyl, phenanthrene) was then challenged in the literature[42–46] and rebutted.[47–48]

Understanding of trends in relative stability of metal complexes is of great importance and often a simple geometric analysis of reported crystal structures is used.[19] For instance, it is known that most (if not all) M(bpy)$_2$ complexes (e.g. of d8 metals) are significantly distorted from the square-planar geometry.[49] On the other hand, replacement of two bpy ligands by four pyridines (this results in M(py)$_4$ complexes) generates a perfect planar coordination sphere with

somewhat rotated py ligands with respect to the coordination plane. Arguably, this could be interpreted as indicating a tendency of these complexes to minimize steric hindrance due to short CH--HC contacts. Validity of this simplistic argument (without exploring the physical nature and strength of the H•••H interaction) however, can be readily questioned when structural data are analyzed, namely the distance between N-atoms in complexes with bpy and py. On average, the intramolecular $d(N--N)$ in $M(bpy)_2$ is about 2.6 Å whereas in $M(py)_4$ the distance between N-atoms of two pyridine ligands is significantly larger, by ~0.2 Å. This observation might explain (again in very simplistic way) the perfect square-planar structures of the $M(py)_4$ complexes because, understandably, there is no way that the bpy molecule could be (i) stretched along the C–C′ bond (linking two pyridine rings) or (ii) twisted along the C–C′ bond to achieve $d(N--N) \cong$ 2.8 Å, as required for the undistorted square planar placement of N-atoms around the central metal ion. In support of the above reasoning one might use the fact that all $M(phen)_2$ complexes are also distorted from the square-planar geometry,[49] even though H-clashes are not present in phen.

Echeverría et al[34] and Danovich et al[35] have demonstrated computationally that there exists very subtle, but stabilizing CH•••HC interactions in alkanes. Very recently McKee and Schleyer have shown that the stability of branched alkanes is related to the correlation effects between the C–H bonds of clashing alkyl groups.[50] Finally, McGrady et al[51–53] have suggested, apart from the typical polar dihydrogen bonding $BH^{\delta-}•••^{\delta+}HN$[54–62], an existence of stabilizing interaction within various homopolar contacts in crystals.

Our main interest in this article is to explore and understand factors that control the relative stability of Zn^{II} based complexes containing ubiquitous bpy ligand, $[Zn(bpy)(H_2O)_4]^{2+}$, $[Zn(bpy)_2(H_2O)_2]^{2+}$ and $[Zn(bpy)_3]^{2+}$ (for simplicity, these complexes will be shown throughout

the text as ZnL, ZnL_2 and ZnL_3). More specifically, all possible interactions will be described (in the minimum energy Zn^{II}-complexes) including donor-acceptor connections (Zn–N, Zn–O) and the intramolecular hydrogen bonds (CH•••N, CH•••O). In addition, the counterintuitive CH•••HC interactions will be characterized based on different approaches. It should be noted that analysis of weak intramolecular bonds is a challenging and far more difficult assignment as compared to the description of typical intermolecular interactions. We will apply four approaches widely used in a description of chemical bonds; (1) QTAIM,[41] (2) the Interacting Quantum Atoms (IQA) energy decomposition scheme,[63–65] (3) the Non-covalent Interactions (NCI) method[66–69] and (4) (ETS-NOCV) energy decomposition scheme.[70–71] It is, to the best of our knowledge, not only the first comprehensive work combining all four methods, but it also characterizes all the intra- and intermolecular interactions in the Zn^{II}-complexes with bpy. Finally, we will very briefly characterize origin of higher stability of non-bonded *trans*-bpy ligand as compared to *cis*-structure.

To facilitate interpretation of interatomic interaction investigated in this work (and to make it convenient to the interested reader) a brief outline of basic theoretical principles of each method employed in this study is provided in the Supporting Information (SI).

2. Computational details

Suitable for energy optimization crystal structures for all forms of octahedral $Zn^{II}L(1)_nL(2)_m$ complexes (L(1) = bpy, L(2) = H_2O (shown further as ZnL_n, $1 \leq n \leq 3$) were obtained from the Cambridge Crystal Structure Database.[49] These structures were optimized using DFT in Amsterdam Density Functional (ADF) 2010 software,[72–74] with X3LYP as the exchange-correlation functional and an augmented triple-ζ basis set with valence-shell polarization (ATZP[75,76]); the COSMO model was used to approximate an aqueous environment implicitly. It

has been shown that X3LYP is suitable for accurate description of weak interactions.[77–79] Calculations using another, dispersion corrected, functional B97-D were also performed.[80] In order to further confirm our conclusions, we also used for selected examples the higher level of computations, i.e. MP2 with the extended triple-ζ basis set 6-311++G(d,p). ETS-NOCV analysis was computed within ADF on the energy-optimized structures (no imaginary frequencies were present).

Wavefunctions for use in QTAIM, IQA and NCI analyses were generated from single point calculations using Gaussian 09, Revision B[81] with the X3LYP functional and 6-311++G(d,p) basis set. For the Gaussian calculations, PCM/UFF was used to model the solvent. Topological analysis, including molecular graph generation and calculation of interaction energies within the IQA approach, was carried out using AIMAll software.[82] NCI analysis was carried out using NCIPlot 2.0,[66] and visualization of the resulting densities was done using VMD 1.9.1.[83]

To perform an IQA analysis, which needs a well-defined second-order density matrix (therefore ruling out DFT-densities), we re-optimized our structures at HF/6-311++G(d,p) with the PCM/UFF solvation model, using Gaussian09c. IQA analysis was performed for selected atoms and interactions on the resulting wavefunctions using AIMAll. All atomic integrations were of accurate integration - the atomic Lagrangian, $L(\Omega)$, deviated from zero only on the fifth decimal place for each atom.

Finally, we have also calculated one-bond $^1J(C–H)$ coupling constants using several functionals (BP86/TZ2P, X3LYP/TZ2P and PBE0/TZ2P) in order to characterize CH--HC close contacts from spectroscopic perspective. It has been proven experimentally and computationally that spin-spin coupling constants are suitable to detect weak bonds; e.g. agostic C–H•••M (M =

metal) interactions, hydrogen bonding interactions (C–H•••D, D = electron donor) or hyperconjugation effects.[84–87]

Fragmentation Schemes. Several fragmentation schemes (for the purposes of ETS-NOCV analyses), needed to extract different types of bonds (Zn–O, Zn–N, C–C) and interatomic interactions (CH•••N, CH•••O and CH•••HC), have been considered and some of them (used for the general ZnL_2 case) are shown in Figure 2. The first scheme is labeled (*7*)-*pyr* and it refers to the use of seven different fragments which include radical pyridine promolecules. The seven-fragment scheme results in (i) four different H_2O molecules, a free Zn^{2+} cation and two pyridine radicals when $Zn(bpy)(H_2O)_4^{2+}$ is analyzed, (ii) two H_2O molecules, four pyridine radicals and a free Zn^{2+} cation in case of ZnL_2 analysis, and (iii) six pyridine radicals and a free Zn^{2+} cation in case of ZnL_3.
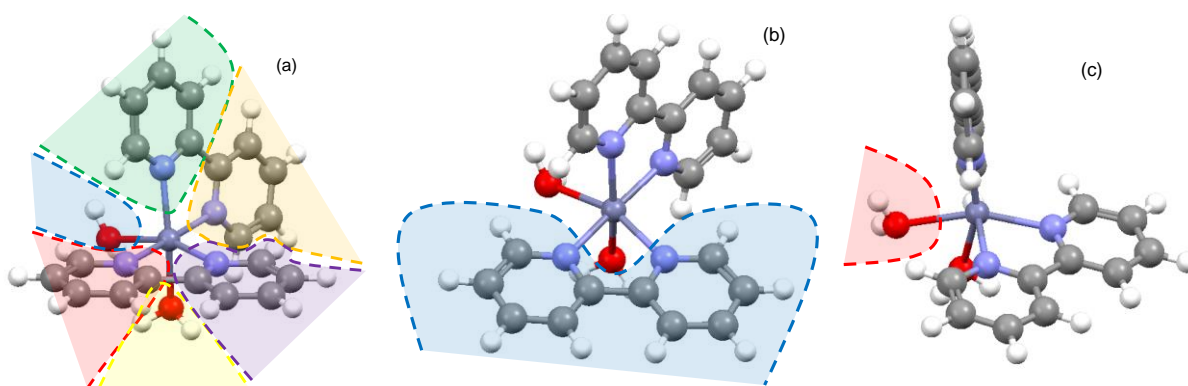
Figure 2. Fragmentation schemes used for ETS-NOCV analysis. (a) (*7*)-*pyr,* (b) (*2*)-*bpy*, and (c) (*2*)-*OH₂*.

We found that such partitioning was most suitable (*i.e.* it provided the most localized NOCV channels) for description of the C–C bond and the intramolecular CH•••HC interactions. Most informative NOCV channels describing the Zn–N and Zn–O coordination bonds and the CH•••O intramolecular interactions were generated from two-fragment schemes, (*2*)-*bpy* and (*2*)-*OH₂*,

where a single bpy ligand or water molecule was separated from a complex, respectively, as shown in Figures 2(b-c) for ZnL_2. It should finally be added that all of our results are qualitatively reproducible across different fragmentation schemes – for example, the interactions seen in (*2*)-*bpy* (or even alternative schemes not included in this work) are seen in (*7*)-*pyr* as well. Similar is true for the remaining interactions.

3. Results and Discussion

3.1. Molecular geometries. We studied the successive coordination of bpy ligands to a Zn^{II} metal ion in aqueous solution and selected structural data obtained for the equilibrium structure of ZnL_2 are shown in Table 1 (structural data for all ZnL_n complexes are included in Table S1 followed by Cartesian coordinates in Tables S2-S4 of the SI). Ball and stick representations, which also show numbering of atoms in the ZnL_n complexes, are shown in Figure S1 of the SI. The average Zn–N bond length (BL) increases by a significant distance of ~0.1 Å, from 2.107 Å in ZnL to 2.218 Å in ZnL_3 and is coupled to a decrease in the N-Zn-N bite angle, from 79.13° in ZnL to on average 74.77° in ZnL_3.

Table 1. Selected structural data for equilibrium geometries of the ZnL_2 complex optimized at the X3LYP/ATZP level of theory in solvent using the COSMO model.

Complex	Bond length (Å)		Bite angle (deg)		Torsion (deg)		Close contacts (Å)	
	Zn–N1	2.153	N1-Zn-N2	77.40	N1-C13-C14-N2	0.31	CH16•••H18C	2.031
	Zn–N2	2.143	N3-Zn-N4	77.48	H16-C15-C13-C14	–0.45	CH32•••H36C	2.036
	Zn–N3	2.149			H18-C17-C14-C13	0.52	CH24•••O6	2.451
ZnL_2	Zn–N4	2.143			N3-C33-C34-N4	1.89	CH42•••O5	2.455
	average:	*2.147*			H32-C31-C33-C34	0.18	CH26•••N2	2.810
	std dev:	*0.005*			H36-C35-C34-C33	0.79	CH8•••N4	2.819
	Zn–O5	2.273						
	Zn–O6	2.276						

All distances between atoms involved in the intramolecular interactions, however, become shorter, e.g. d(CH--HC) decreases from 2.048 Å in ZnL to ~2.034 and ~2.010 Å in ZnL_2 and ZnL_3, respectively, whereas d(CH--O) decreases from ~2.544 Å in ZnL to ~2.453 Å in ZnL_2. At the same time, the ligand molecules remain virtually planar in the ZnL_n complexes, e.g. the absolute maximum and minimum values of N_1-C_2-$C_{2'}$-$N_{1'}$ dihedral angle of 1.89 and 0.31°, respectively, were found.

3.2. QTAIM-based interpretation of the electron density topology. Figure 3 shows the molecular graph of ZnL_2 (ZnL and ZnL_3 are shown in Figure S2 of the SI). Since atomic interaction line (AIL) represents a 'bridge of density' or just a line of maximum density that links two atoms (a topological property of electron density which can be defined, in the form of operator, as a Dirac observable, making the AIL the measurable expectation value of a quantum
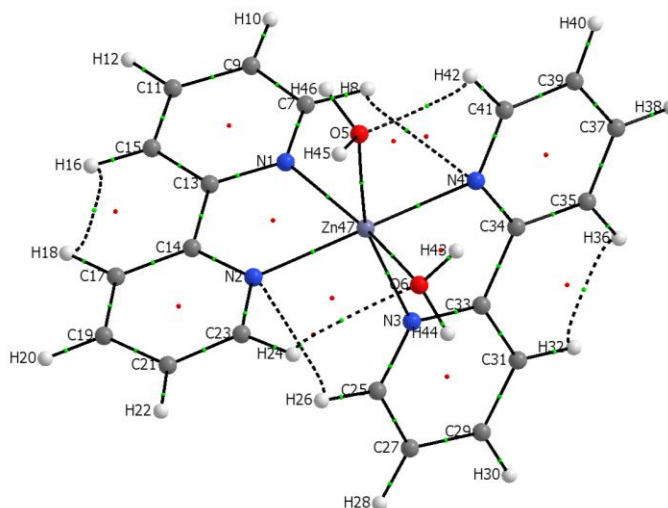
Figure 3. A QTAIM molecular graph of ZnL_2.

mechanical operator[31]) it is undistinguishable for classical covalent or coordination bonds (they are shown as solid lines) or closed-shell intramolecular interactions (shown as dashed lines) for (i) CH•••O interactions in ZnL and ZnL_2, (ii) CH•••N interactions in ZnL_2 and ZnL_3 and (iii) CH•••HC interactions between the 3,3′-H atoms in all ZnL_n complexes.
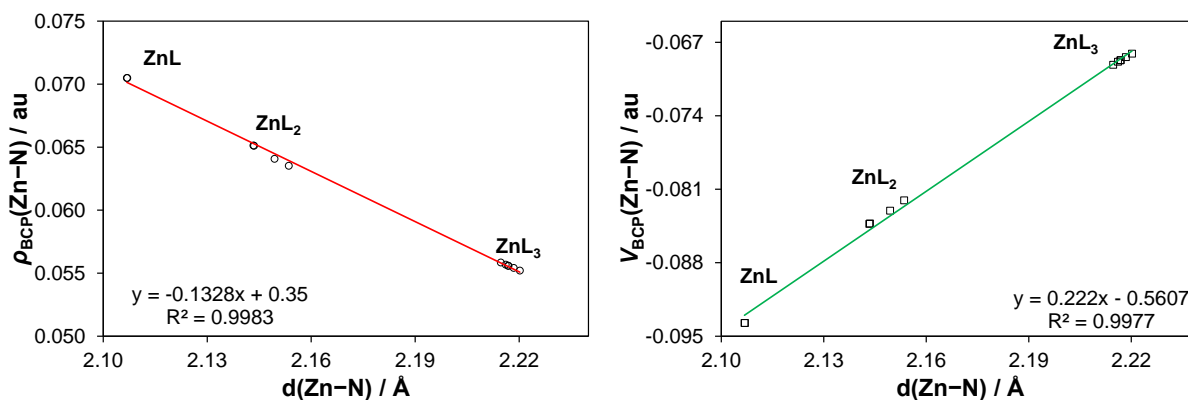
Coordination bonds. Topological properties at BCPs for Zn–N and Zn–OH$_2$ bonds in ZnL$_2$

are collected in Table 2 (data for ZnL$_n$ are included in Table S5 of the SI). It is seen that ρ_{BCP} is

small (0.0405 a.u. $< \rho(r) <$ 0.0705 a.u.) and $\nabla^2\rho_{BCP}$ is small and positive (0.1519 a.u. $< \nabla^2\rho(r) <$

0.2522 a.u.) indicating a "closed shell" character of the coordination bonds.[88] The local electron

potential energy density $V(r)$ dominates the local electron kinetic energy density, $G(r)$, in these

two coordination bonds and results in the overall negative (although small) value of the total

energy density, $H(r) = G(r) + V(r)$. This strongly points out at a significant covalent

contribution,[88-93] hence also recovers a 'classical' notion of a coordination bond where a donor

atom (here N and O) shares a pair of electrons with the central metal ion. One can also use the

$|V(r)|/G(r)$ ratio as another useful description;[88,94] $|V(r)|/G(r) < 1$ is characteristic of a typical

ionic interaction and $|V(r)|/G(r) > 2$ is diagnostic of a 'classical' covalent interaction. Taking all

these criteria into consideration, the QTAIM-defined topological properties at BCPs indicate a

mixed (largely ionic with significant covalent component) character of these coordination bonds,

also because $1 < |V(r)|/G(r) < 1.1$.

To facilitate our comparative studies we have decided to investigate the variation in

topological properties with a change in the interatomic distances, d(A--B). Relationships for the

electron density, ρ_{BCP}, and the potential energy density, V_{BCP}, are shown in Figure 4 (plots for

$\nabla^2\rho_{BCP}$, G_{BCP}, H_{BCP}, and $|V_{BCP}|/G_{BCP}$ are shown in Figure S3 of the SI; relationships obtained for

bonds involving water molecules are shown in Figure S4 of the SI). We observe that ρ_{BCP}

decreases while V_{BCP} becomes more positive when d(Zn--L) increases; this (and relationships

shown in Figure S4 of the SI) indicates weakening of coordination bonds from ZnL to ZnL$_3$, the

latter being most crowded.

Table 2. Topological data at the BCP for all coordination bonds in ZnL_2 (L = 2,2′-bipyridyl) optimized at X3LYP[a]

Complex	Atoms	$\rho(r)$	$\nabla^2\rho(r)$	$V(r)$	$G(r)$	$H(r)$	$|V(r)|/G(r)$
ZnL$_2$	Zn–N1	0.0635	0.2191	−0.0821	0.0684	−0.0136	1.1993
	Zn–N2	0.0651	0.2245	−0.0843	0.0702	−0.0141	1.2004
	Zn–N3	0.0641	0.2221	−0.0830	0.0693	−0.0138	1.1986
	Zn–N4	0.0651	0.2246	−0.0843	0.0702	−0.0141	1.2003
	Average	*0.0645*	*0.2226*	*−0.0834*	*0.0695*	*−0.0139*	*1.1996*
	Zn-O5	0.0408	0.1533	−0.0503	0.0443	−0.0060	1.1353
	Zn–O6	0.0405	0.1519	−0.0499	0.0439	−0.0059	1.1351
	Average	*0.0407*	*0.1526*	*−0.0501*	*0.0441*	*−0.0060*	*1.1352*

[a] $\rho(r)$, $\nabla^2\rho(r)$, $V(r)$, $G(r)$, and $H(r)$ - all in atomic units.

Figure 4. Relationships between bond lengths and indicated topological properties at the BCP for Zn–N bonds.

Intramolecular interactions. Selected topological properties for intramolecular interactions in the ZnL_2 complex are included in Table 3 (data for ZnL_n are presented in Table S6 of the SI) and examples of trends obtained for the CH•••HC interactions are shown in Figure 5. For all intramolecular interactions we observe (i) an increase in ρ_{BCP} and $|V_{BCP}|$ as the interatomic distance shortens from ZnL to ZnL_3, and (ii) predominant closed-shell character (G_{BCP} dominates, the ratio $|V_{BCP}|/G_{BCP} < 1$, and since $\nabla^2\rho_{BCP} > 0$, the electron density is concentrated to the respective atomic basins rather than being contracted towards and along the interatomic surface, the latter results in $\nabla^2\rho_{BCP} < 0$ observed for covalent bonds). Moreover, as opposed to

the coordination bonds, the largest ρ_{BCP} is observed in ZnL_3 which suggests that the CH•••O, CH•••N, CH•••HC interactions are strongest in the most crowded complex.

Table 3. Topological data at the BCP for all intramolecular interactions in ZnL_2 optimized at X3LYP[a]

Complex	Atoms	$\rho(r)$	$\nabla^2\rho(r)$	$V(r)$	$G(r)$	$H(r)$	$\|V(r)\|/G(r)$
	CH42–O5	0.0098	0.0358	–0.0063	0.00760	0.0013	0.8263
	CH24–O6	0.0099	0.0361	–0.0064	0.0077	0.0013	0.8274
	Average	*0.0099*	*0.0359*	*–0.0063*	*0.0077*	*0.0013*	*0.8269*
	CH26–N2	0.0060	0.0202	–0.0034	0.0042	0.0008	0.8072
ZnL_2	CH8–N4	0.0059	0.0199	–0.0034	0.0042	0.0008	0.8067
	Average	*0.0060*	*0.0200*	*–0.0034*	*0.0042*	*0.0008*	*0.8069*
	CH16–H18C	0.0118	0.0452	–0.0067	0.0090	0.0023	0.7478
	CH36–H32C	0.0117	0.0448	–0.0067	0.0090	0.0023	0.7473
	Average	*0.0118*	*0.0450*	*–0.0067*	*0.0090*	*0.0023*	*0.7475*

[a] $\rho(r)$, $\nabla^2\rho(r)$, $V(r)$, $G(r)$, and $H(r)$ - all in atomic units.

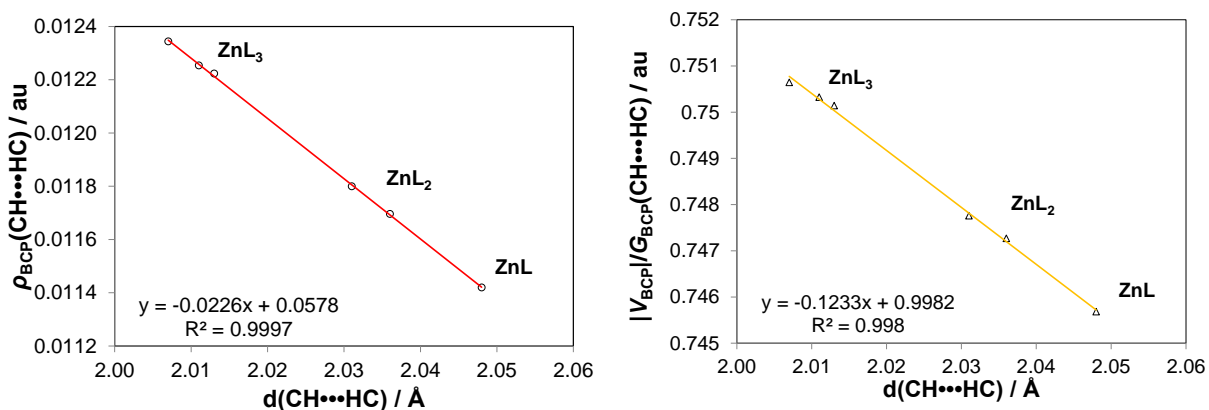**Figure 5**. Relationships between indicated topological properties at the BCP and d(CH--HC) in ZnL_n.

Our results agree with the topological analysis at BCP obtained from experimental data which was performed by (i) Flaig *et al*[95] (this involved weak and strong inter- and intramolecular H-bonds in aminoacids) and (ii) Espinosa *et al*[96] (they investigated the X–H•••O interactions in over 83 structures). This clearly indicates that the topological properties at BCPs exhibit the same universal relationship with d(A--B), regardless if theoretical or experimental data are used.

We conclude this section by stating that the electron density distribution along the AIL of the CH•••HC interaction, as well as the change in the energy densities at BCPs upon additional ligand coordination, is qualitatively identical to those observed for closed-shell bonding interactions (CH•••O, CH•••N).

3.3. IQA Energy Decomposition Analysis. A QTAIM-defined bond path indicates the presence of a privileged quantum-mechanical exchange channel[32] and it always makes a stabilizing contribution. However, to interpret the physical nature of an interatomic interaction and its local contribution (either stabilizing or not) to the overall energy of a molecule, other energy contributions should be considered.[51,52,55,56,97,98] Therefore, we decided to use the computationally expensive but highly useful IQA. One might recall that IQA defines the interaction between two atoms as a competing contribution made by classical components (interaction energies between electrons and nuclei as well as Coulombic interaction between electrons of atoms A and B) conveniently combined as V_{cl}^{AB}, and quantum-mechanical contribution, as V_{XC}^{AB}. Since the IQA scheme is not suitable for DFT wavefunctions,[32,64,65] we re-optimized our complexes at the HF level. Note that the quantum-mechanical energy term V_{XC}^{AB} computed at the HF level does not have the correlation term, but our main interest is in a qualitative description of these interactions and according to previous reports[32,64,65] this can be achieved at the HF level, even with modest basis sets.

We will analyze the IQA results primarily for ZnL_2, since all intramolecular interactions, CH•••O, CH•••N and CH•••HC, are present only in this complex. The interaction energy, $E_{int}^{AB} = V_{cl}^{AB} + V_{XC}^{AB}$, for (i) all relevant intramolecular interactions, (ii) coordination Zn–N and Zn–O bonds, (iii) the covalent C–C bond, and (iv) the intramolecular non-bonded N-atoms of the

ligand are shown in Table 4 (a full set of data for all ZnL_n complexes is provided in Table S7 of the SI).

When the relative values of $E_{\text{int}}^{\text{AB}}$ are considered, we found that the Zn–N and Zn–O bonds are characterized by the largest $|E_{\text{int}}^{\text{AB}}|$ values, about −390 and −300 kcal mol^{-1}, respectively, followed by the C–C bond for which $|E_{\text{int}}^{\text{C,C}}|$ is about 100 kcal mol^{-1} smaller when compared with Zn–O. This is somewhat an unexpected result and it fully justifies further studies (involving more metal complexes) to explore and understand that better – one must remember, however, that the IQA-defined interaction energy must not be confused with the bond-dissociation or binding energy. The latter is defined in IQA as $E_{\text{bind}}^{\text{AB}} = \Delta E_{\text{self}}^{\text{A}} + \Delta E_{\text{self}}^{\text{B}} + E_{\text{int}}^{\text{AB}}$, where ΔE_{self} is the change in self-energy (intra-atomic energy) in relation to a suitable reference frame. In other words, the interaction energy combined with the changes *within* an atomic basin gives a quantity more related to the bond dissociation energy. Regarding atoms in polyatomic molecules, such as the present case, estimation of the change in E_{Self} and its physical interpretation in particular,

Table 4. Decomposition of two-bodied interaction energies within the IQA framework for all relevant interactions in ZnL$_2$ complexes with 2,2′-bipyridyl (L).

Atoms	d(A–B)	$V_{\text{ne}}^{\text{AB}}$	$V_{\text{en}}^{\text{AB}}$	$V_{\text{nn}}^{\text{AB}}$	V_{C}^{AB}	$V_{\text{cl}}^{\text{AB}}$	$V_{\text{XC [a]}}^{\text{AB}}$	$E_{\text{Int}}^{\text{AB}}$	$V_{\text{XC}}^{\text{AB}} / E_{\text{Int}}^{\text{AB}}$
	Å	a.u.	a.u.	a.u.	a.u.	kcal·mol^{-1}	kcal·mol^{-1}	kcal·mol^{-1}	
CH•••HC	2.050	−0.2488	−0.2488	0.2581	0.239	−0.2	−2.5	−2.7	0.92
CH•••O	2.502	−1.7656	−1.7656	1.6917	1.8195	−12.5	−3.3	−15.7	0.21
CH•••N	2.879	−1.3988	−1.3988	1.2866	1.4953	−9.9	−1.6	−11.6	0.14
C–C	1.497	−11.4030	−11.4030	12.7264	10.233	96.3	−193.4	−97.2	1.99
Zn–N1	2.183	−55.1408	−55.1408	50.9086	58.8099	−353.4	−36.7	−390.1	0.09
Zn–N2	2.182	−55.1524	−55.1524	50.9243	58.8145	−355.1	−36.8	−391.9	0.09
Zn–O6	2.236	−59.7008	−59.7008	56.7947	62.1597	−280.5	−23.0	−303.5	0.08
N1•••N2	2.676	−11.8153	−11.8153	9.6902	14.4061	292.3	−7.2	285.0	−0.03

[a] Note that only exchange energy is used to calculate full $E_{\text{XC}}^{\text{AB}}$ term because of the Hartree-Fock approximation.

becomes, in principle, an impossible task. This is because (i) an atom which is identical in every physical and chemical manner but without the presence of the specific interatomic interaction needs to be found, (ii) definition of such atom in molecule is ambiguous as pointed out by Parr, Ayers and Nalewajski[99] (though from the experimental point of view the atoms are the real objects, as correctly rebutted by Matta and Bader,[100] providing QTAIM-predicted atomic properties) and (iii) in complex molecular environment, where many interactions occur simultaneously, it is difficult to determine exact information, such as binding energy, about any particular single interaction.[101]

The interaction energy between N-atoms of the bipyridyl ligand found from IQA is +285.1 kcal·mol^{-1} and thus recovers our classical notion of strong repulsion between them.

Regarding intramolecular interactions, we found the following trend $|E_{\text{int}}^{\text{H,O}}| > |E_{\text{int}}^{\text{H,N}}| \gg |E_{\text{int}}^{\text{H,H}}|$ which appears to corroborate with a general notion when CH•••O and CH•••N are concerned (due to the difference in electronegativity, the latter interaction is expected to be weaker). Importantly, the IQA analysis at the HF level does also predict the CH•••HC interaction to be of stabilizing nature as $E_{\text{int}}^{\text{H14,H18}}$ = –2.7 kcal·mol^{-1} is certainly not negligible. In order to obtain more accurate results, we decided to optimize ZnL at the MP2 level. The computed value of $E_{\text{int}}^{\text{H14,H18}}$ was –2.1 kcal mol^{-1} which is in support of the above overall conclusions arrived at from the HF calculations. It is important to emphasize that we do not claim that the overall binding energy of CH•••HC is negative; we have identified stabilizing, local, electron exchange-correlation channel stemming from the CH•••HC interaction. Similar electron exchange contributions were found by Pendás et al[32] for other set of molecules containing CH--HC contacts, despite the fact that the IQA-defined binding energy appeared to be positive (overall repulsive interaction) due to significant increase in the self-deformation energies of H-atoms.

We focus now on the energy partitioning terms (see Eq 8 in the SI) which describe the physical nature of an interaction, namely whether it might be seen mainly of electrostatic, $V_{cl}^{AB} << V_{XC}^{AB}$, or quantum mechanical exchange origin. The latter case can be seen as a process of delocalization of electrons between atoms involved. It is seen in Table 4 that all non-covalent bonds and intramolecular interactions which show AILs can be characterized as of a strong ionic nature except CH•••HC, e.g. in case of Zn–OH$_2$, the $V_{cl}^{Zn,O}$ term makes over 12 times larger stabilizing contribution than $V_{XC}^{Zn,O}$. The CH•••O and CH•••N interactions show a chemical nature similar to the Zn–N and Zn–O bonds in that the stabilizing contribution to E_{int}^{AB} comes mainly from V_{cl}^{AB} with the V_{cl}^{AB}/V_{XC}^{AB} ratio approaching 6 and 4 for CH•••N and CH•••O, respectively.

We note with interest that the $V_{cl}^{H,H}$ term is very small and negative (the overall IQA-defined electrostatic CH•••HC interaction is not repulsive at the HF level). However, at the MP2 level of theory, the $V_{cl}^{H14,H18}$ term became slightly positive, +1.0 kcal mol^{-1}, but it was compensated over by the $V_{XC}^{H14,H18}$ term, −3.0 kcal mol^{-1} (additional data, obtained from the SPC at the MP2 level on the DFT-structures, are presented in Table S8 in the SI); this contradicts the classical and mainly MM-based notion of highly repulsive H-clashes in these complexes. Moreover, the ratio V_{XC}^{AB}/V_{int}^{AB} of ~0.92 (or ~1.48 at MP2) is very different when compared with CH•••N and CH•••O interactions. This suggests that the physical nature of the CH•••HC interaction is unique among those studied here and the QTAIM-based criteria derived by Popelier[102] for hydrogen bonds is not applicable. We do not claim here that the local electronic exchange stabilization between the 3,3′-hydrogen atoms is formed spontaneously. It is obvious that the 3,3′-hydrogen atoms are in

the forced-to-be clash because of the formation of orders of magnitude stronger coordination bonds. In other words, very strong affinity of metal ion to the N-atoms of bpy overrides preferential conformational state of the ligand (s-*trans*) and is forcing bpy to change to s-*cis* conformation. The associated energy penalty of this conformational change is about 4 kcal mol^{-1} in comparison with hundreds of kcal mol^{-1} released due to the interaction energy associated with the formation of strong coordination bonds (Table 4); also rotational energy barrier (less than 10 kcal mol^{-1}) is by far smaller than the overall energy gain on complex formation.

We have also investigated selected interactions in the free ligand bpy. From considering just the strength of these interactions, we concluded that the preferential conformational state of bpy is controlled by (i) highly repulsive N--N contact (this is the interaction which makes the s-*cis* conformer energetically unstable) and (ii) two CH•••N interactions which re-enforce the stability of the s-*trans* conformer – more details are included in the SI."

Considering a typical covalent bond between 2,2′-carbons forming a bridge between pyridyl rings, the interaction energy contains a large repulsive electrostatic term (96.3 kcal·mol^{-1}) which is compensated over by stabilization due to 'sharing' of electrons, $V_{XC}^{C,C} = -193.4$ kcal·mol^{-1}. On the other hand, the N•••N interaction is characterized almost entirely by extremely large electrostatic repulsion, $V_{cl}^{N,N} = +292.3$ kcal·mol^{-1} and this correlates very well with the QTAIM analysis where the bond path between these N-atoms is not observed.

Let us consider now the last column in Table 4, were we placed the $V_{XC}^{AB} / E_{int}^{AB}$ ratio, called further the exchange-interaction ratio, EIR. Because V_{XC}^{AB} is always negative, the sign of EIR can be used to identify an interatomic interaction as overall either (i) locally stabilizing when EIR > 0

(e.g. positive values of EIR is observed here for all intramolecular interactions), or (ii) locally destabilizing, as we observe here for the N•••N interaction for which EIR < 0.

The analysis of data seen in Table 4, in combination with EIR, leads us to another observation. It appears that the variation in the EIR values (only when EIR > 0) might correlate with a classical interpretation of a strong covalent, ionic, or intermediate interaction. There are two possible cases for which EIR remains positive, namely when (i) $V_{\text{cl}}^{\text{AB}} < 0$, or (ii) for $V_{\text{cl}}^{\text{AB}} > 0$ when $|V_{\text{XC}}^{\text{AB}}| > V_{\text{cl}}^{\text{AB}}$. For 0 < EIR << 1 (when $|V_{\text{XC}}^{\text{AB}}| << |E_{\text{int}}^{\text{AB}}|$) an interaction is dominated by electrostatic terms (the smaller EIR the larger degree of iconic character is observed) whereas a value well above 1 (when $|V_{\text{XC}}^{\text{AB}}| >> |E_{\text{int}}^{\text{AB}}|$) points at a predominantly or fully classical covalent bond. For instance, in the case of the Zn–O and Zn–N bonds as well as CH•••N and CH•••O interactions, where we observe a predominant ionic character ($V_{\text{cl}}^{\text{AB}}$ significantly dominates the quantum term, $V_{\text{XC}}^{\text{AB}}$) the EIR << 1. On the other hand, EIR is almost 2 for the C–C bond, recovering its classical covalent character fully.

3.4. NCI Analysis. NCI discovers and quantifies non-covalent interactions from the analysis of $\rho(r)$ in large interatomic volumes and, importantly, is able to describe interatomic interactions also in the absence of the QTAIM-defined density critical points, such as BCP or RCP.

Figure 6 shows isosurfaces for all non-covalent interactions in ZnL_2; isosurfaces for individual interactions in ZnL_2 are shown in Figure S5 of the SI, whereas full sets of isosurfaces in ZnL and ZnL_3 are shown in Figure S6 of the SI. The color of isosurfaces depends on the sign of the λ_2 eigenvalue, giving an indication of the nature of the interaction (the color scheme used, from blue, through green to red, reflects the following range –0.07 a.u. < sign(λ_2) × ρ < 0.03 a.u. and it is implemented consistently throughout). For regions where $\lambda_2 > 0$ (red isosurfaces) a local

19
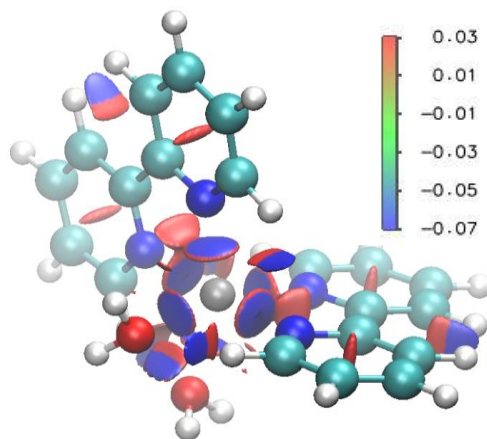
Figure 6. NCI isosurfaces of ZnL_2. The surfaces describe the reduced density gradient at an isovalue of 0.5 a.u. The surfaces are colored on a blue-green-red scale according to values of $\text{sign}(\lambda_2)\rho$, ranging from -0.07 to 0.03 a.u.

depletion of the electron density occurs which might be linked with repulsive forces or steric strain regions, whereas for $\lambda_2 < 0$ (blue color is used), locally increased electron density exists and this has been interpreted as attractive interatomic interaction.[66,68,103]

The Zn–N and Zn–O bonds are shown as large blue discs surrounded by a red ring of depletion. Similar phenomenon has been recently noted during the study of intermolecular H-bonds formed between two water molecules.[69] The red ring was observed at intermolecular distances, $d(HO\text{–}H\text{-}\text{-}OH_2)$, shorter than that of the dimer's minimum energy on the potential energy surface; it has been interpreted as repulsion caused by steric crowding.[69] Here, particularly when combined with a large red disc between N-atoms (a signature of density depletion due to large electrostatic repulsion) it strongly points at strained coordination sphere around the central metal ion.

NCI isosurfaces do not provide any definite evidence that the interatomic regions of intramolecular interactions (CH•••O, CH•••N and CH•••HC) are strained. Note that the electron

accumulation (blue region) is placed directly in the bonding region of the interacting atoms (H•••N, H•••O, and H•••H) whereas a single red region between N-atoms of bpy is observed. The electron density depletion observed outside the bonding region of the H•••N/O and H•••H interactions is related to the formation of the additional ring with a prerequisite ring critical point ($\rho_{RCP} < \rho_{BCP}$, hence red region is observed). In support of our interpretation, one might use the IRC[104] path for electro-cyclization of butadiene with ELF/NCI snapshots of reactants, transition state, and products.[68] A single stabilizing interaction was initially present between two terminal carbon atoms. When a transitional stage was reached, the NCI analysis showed the two-color isosurface (similar to what we observe) which bifurcated along the reaction coordinate into the C−C bond and the red isosurface (called a ring tension[68]) in the center of the ring.

Selected NCI-plots (reduced density gradient, RDG, against sign(λ_2)ρ), which can be seen as signatures of non-covalent interactions in ZnL_2, are shown in Figure 7 (NCI-plots for other complexes are shown in Figures S7-S9 of the SI). The values of $\rho(r)$, where each trough approaches zero of the RDG scale, are known as NCI Interaction Critical Points (ICPs).[68] The larger absolute values of $\rho(r)$ at each ICP associated with density accumulation (where sign(λ_2)ρ < 0) the stronger stabilizing noncovalent interaction is observed. The larger absolute values of $\rho(r)$ at each ICP the stronger e.g. stabilizing non-covalent interaction is observed. For instance, Zn–N shows $(-)\rho_{ICP}^{Zn,N}$ more negative, by 0.02387 a.u., than $(-)\rho_{ICP}^{Zn,O}$ and this corroborates well with the QTAIM and IQA findings (from analysis of either ρ_{BCP} or E_{int}^{AB}) that the Zn–O bond is weaker. ICPs at ~0 indicate a weak classical van der Waals interaction (example of the NCI plot representing a weak interaction observed for the methane dimer is shown in Figure S10 of the SI), but none of the intramolecular interaction discussed here falls under this kind of interaction;

they all have a significant exchange-correlation term. The values of $\text{sign}(\lambda_2)\rho$ at each ICP, $\rho_{\text{ICP}}^{\text{AB}}$,

for selected non-covalent interactions in ZnL_2 are shown in Table 5 (data for all complexes are

shown in Table S9 of the SI); the ICPs associated with accumulation and depletion are labeled $(-)\rho_{\text{ICP}}^{\text{AB}}$, and $(+)\rho_{\text{ICP}}^{\text{AB}}$, respectively.

The values of $(+)\rho_{\text{ICP}}^{\text{AB}}$ and ρ_{RCP} (from QTAIM) are almost identical, e.g. $(+)\rho_{\text{ICP}}^{\text{H,H}} = 0.01104$

and $\rho_{\text{RCP}}^{\text{H,H}} = 0.01105$ or $(+)\rho_{\text{ICP}}^{\text{H,O}} = 0.00768$ and $\rho_{\text{RCP}}^{\text{H,O}} = 0.00765$, all in ZnL_2. This finding points

at previously reported interpretations of RCP regions as either ring-tension,[68] or destabilizing

electron "voids".[103] Interpreting the RCP regions as purely destabilizing, however, does not

seem to be convincing. A reported study[105] showed a good correlation between densities at BCP

and RCP and the strength of an intramolecular hydrogen bond, or larger values of ρ_{RCP} have been

correlated with increased aromaticity;[106,107] a characteristic single trough is observed for the RCP
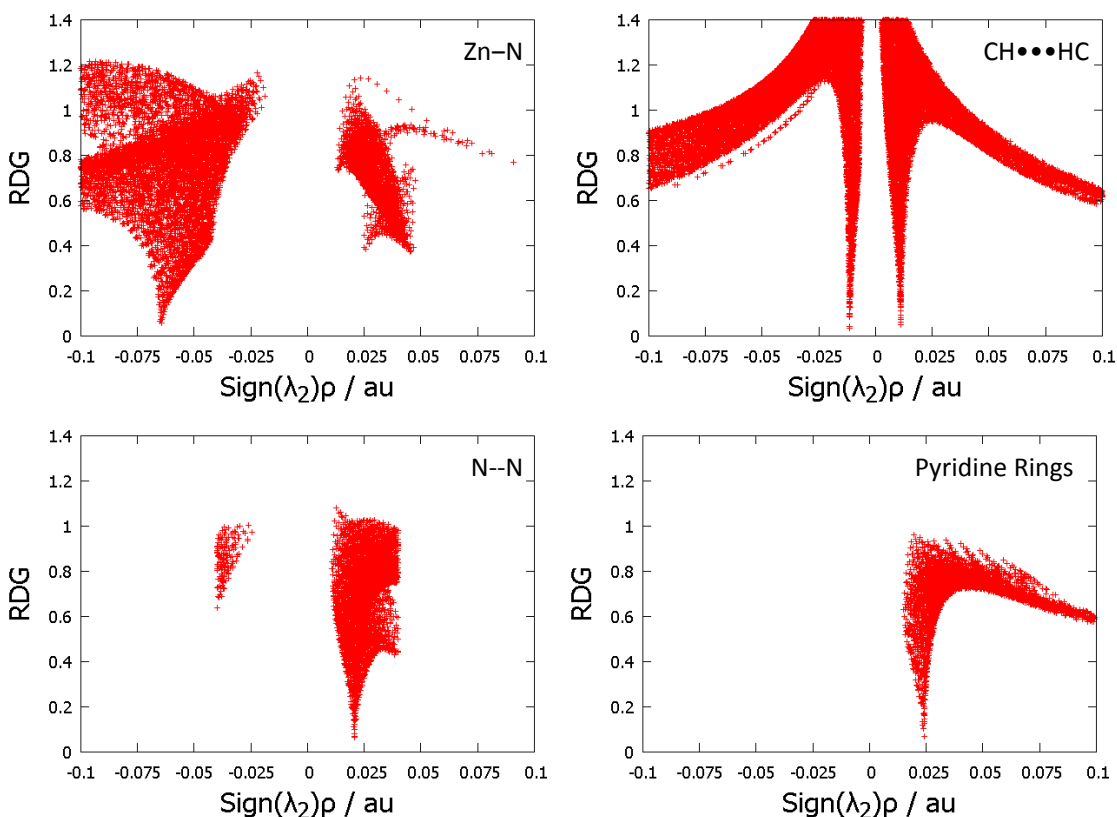
Figure 7. NCI-plots for indicated intramolecular interactions in ZnL_2.

of a pyridine ring which is placed, as one would expect, in the positive range of sign(λ_2)ρ (Figure 7). In our opinion, the $(+)\rho_{ICP}^{AB}$ values resulting from the various intramolecular interactions showing an AIL should be related to the polyatomic interaction of the entire ring rather than be only attributed to e.g. steric repulsion for a diatomic intramolecular interaction.

A very interesting NCI plot was obtained for the N•••N interaction where two troughs, representing large depletion and small accumulation, are observed (a large red isosurface is seen in Figure 6). This overall picture compares surprisingly well with IQA analysis of this interaction where electrostatic repulsion is dominating, $V_{cl}^{N,N} >> V_{XC}^{N,N}$.

Table 5. NCI data for all ZnL_2 coordination bonds and intramolecular interactions.

Interaction	$(-)\rho_{ICP}^{AB}$ [a]	$(+)\rho_{ICP}^{AB}$ [a]
Zn–N	–0.0645	
Zn–O	–0.0406	
CH•••HC	–0.0116	0.0110
CH•••O	–0.0101	0.0077
CH•••N	–0.0060	0.0058
N•••N		0.0208
Pyridine Rings		0.0240

[a] In a.u.

In summary, the NCI analysis agrees very well with interpretation and conclusions arrived at from QTAIM and IQA data. In addition, and importantly, it does not provide any evidence of steric strain in the interatomic region of the CH•••HC interaction or as being van der Waals type of interaction, but it points at the coordination sphere as a place of significant steric strain.

3.5. ETS-NOCV-based analysis of deformation densities. ETS-NOCV differs significantly from all three techniques discussed above as it involves representation based on fragment molecular orbitals rather than real space density distributions. A particularly attractive feature of this method is in the visualization of molecular regions from which electrons were either removed or gained when fragments form chemical bonding. The examples of dominant NOCV deformation density channels for Zn–N and Zn–O bonds in ZnL are shown in Figure 8 (see also Figure S11 in the SI where NOCV channels for coordination bonds in ZnL_2 and ZnL_3 are shown). Blue and red colors indicate accumulation and depletion, respectively, of the electron density and the NOCV-based channels, such as in Figure 8, can be seen as textbook examples of the classical interpretation of coordination bonds, where ligands donate electron density to available hybridized *sd*-orbitals of the central metal ion.

A predominant single covalent bond between C_2–$C_{2'}$ joining the two pyridyl rings can be deduced from the shape of $\Delta\rho_l$ in Figure 9a (it can be ascribed to traditional σ-contribution) and the corresponding large negative ΔE_{orb} value –239.5 kcal mol^{-1} which is about ten times larger (in absolute value) when compared to π-stabilization shown in Figure 9b ($\Delta\rho_k$ for ZnL_2 are presented in Figure S12 of the SI). These NOCV-based channels demonstrate that electron density is accumulated within the *bonding* interatomic region and is evenly depleted mainly from the *non-bonding* region of the carbon atoms.

Two charge density accumulations describe intramolecular CH•••O interaction, Figure 10, where (i) ionic character is related to typical σ-donation from the lone electron pair of oxygen to the empty σ*(C–H) and it is displayed by a dominant component (ΔE_{orb} = –1.8 kcal mol^{-1}, part a in Fig. 10) and (ii) significant covalency of CH•••O interaction, i.e. charge accumulation in the H•••O interatomic region shown by a supporting channel with ΔE_{orb} = –0.8 kcal mol^{-1}, Fig. 10b.

An important role of the covalency in the hydrogen bonded systems was noticed and extensively studied by Grabowski.[108] The NOCV-recovered type of interaction is also consistent with
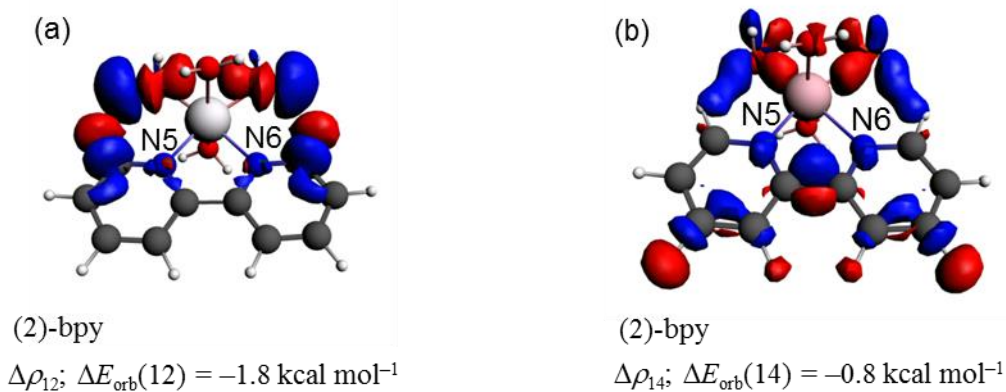

(2)-bpy
$\Delta\rho_1$; $\Delta E_{orb}(1) = -37.7$ kcal mol^{-1}

(2)-OH$_2$
$\Delta\rho_2$; $\Delta E_{orb}(2) = -11.8$ kcal mol^{-1}
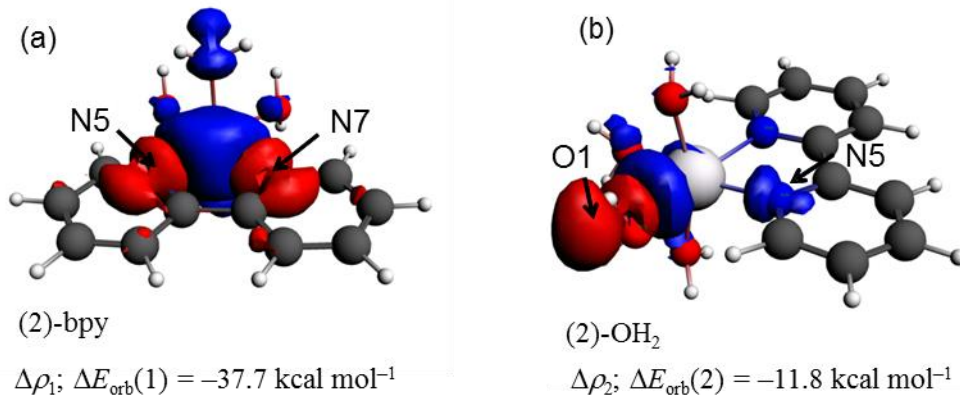
Figure 8. Representative NOCV-based deformation densities for (a) Zn–N and (b) Zn–O coordination bonds in ZnL.

(7)-pyr, $\alpha + \beta$
$\Delta\rho_1$; $\Delta E_{orb}(1) = -239.5$ kcal mol^{-1}

(7)-pyr, $\alpha + \beta$
$\Delta\rho_2$; $\Delta E_{orb}(2) = -24.0$ kcal mol^{-1}
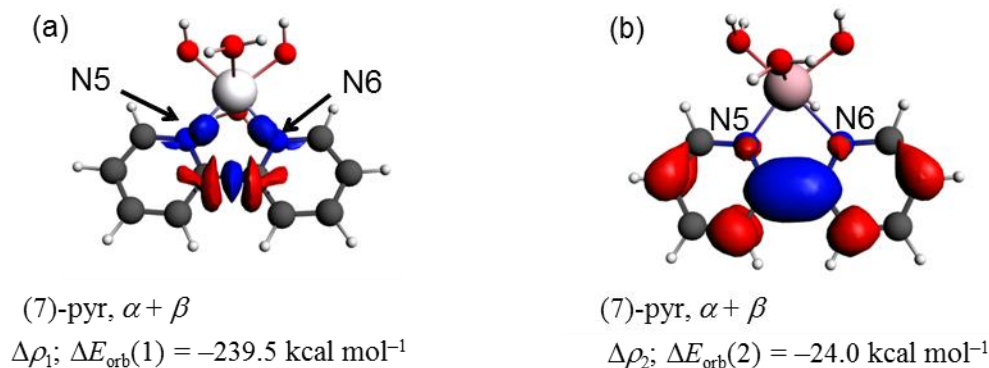
Figure 9. Characteristic NOCV-based deformation densities obtained for the C$_2$–C$_{2'}$ bridge in ZnL.

(2)-bpy
$\Delta\rho_{12}$; $\Delta E_{orb}(12) = -1.8$ kcal mol^{-1}

(2)-bpy
$\Delta\rho_{14}$; $\Delta E_{orb}(14) = -0.8$ kcal mol^{-1}

Figure 10. NOCV-based deformation densities for the CH•••O interactions in ZnL.

Popelier's QTAIM-based criteria[102] defining a classical H-bond. The covalent-like deformation density (Figure 10b) corresponds well with (i) the topological representation of a bonding interaction, a bridge of maximum electron density between H and O atoms, AIL, and (ii) $V_{XC}^{H,O}$ of IQA analysis. In general, NOCV-based deformation density channels predict a dominant ionic character of the CH•••O interaction and this correlates very well with the IQA analysis, $V_{cl}^{H,O} \gg V_{XC}^{H,O}$.

(a)

N5   N6

(7)-pyr, $\alpha + \beta$
$\Delta\rho_{23}$; $\Delta E_{orb}(23) = -1.8$ kcal mol^{-1}

(b)

N5   N6

(7)-pyr, $\alpha + \beta$
$\Delta\rho_{21}$; $\Delta E_{orb}(21) = -2.5$ kcal mol^{-1}
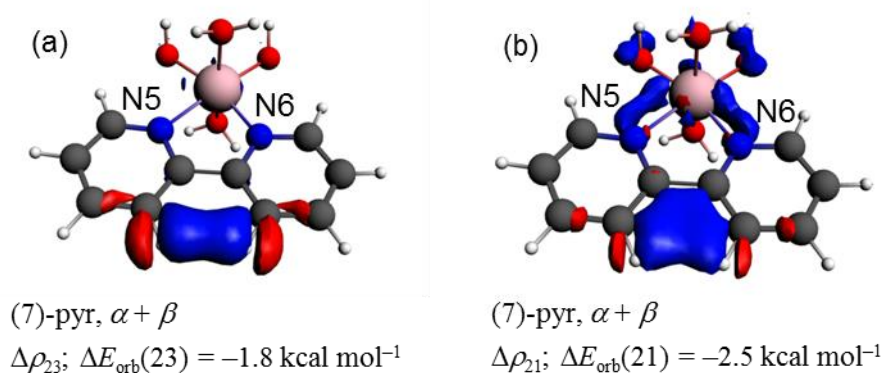
Figure 11. NOCV-based deformation densities for the CH•••HC interactions in ZnL.

Regarding the CH•••HC interaction, the first component, with $\Delta E_{orb} = -1.8$ kcal mol^{-1} in Figure 11a (full set of $\Delta\rho_k$ for all intramolecular interactions in ZnL$_2$ is shown in Figure S13 of the SI), shows a transfer of electron density from the non-bonding to the bonding region between the H-atoms; this charge deformation resembles the covalent-like NOCV channel obtained for CH•••O shown in Figure 10b. The second and unique type of deformation density channel, with $\Delta E_{orb} = -2.5$ kcal mol^{-1} shown in Figure 11b, illustrates multi-atomic-basin density accumulation and involves all atoms in the 6-membered ring. Interestingly, the main depletion of the charge appears to be again the non-bonding region of atomic basins of the H-atoms involved in this

interaction. These two NOCV contributions can be compared with the topology of the electron density in the form of AIL in the case of $\Delta\rho_{23}$ (part a in Figure 11), while $\Delta\rho_{21}$ (part b in Figure 11) compares well with the increased density and gradient ρ paths associated with the formation of a ring critical point on the molecular graph. Moreover, the observed NOCV contributions strongly indicate a predominant covalent (spin-pairing) character of the CH•••HC interactions and this correlates well with the IQA interaction energy components, in absolute values $V_{cl}^{H,H} <<$ $V_{XC}^{H,H}$. Qualitatively, one can state in the language of molecular orbitals, that formation of CH-- HC contacts gives rise to significant polarization of C–H bonds (mixing of σ/σ^*(C–H) within the same C–H unit), what leads to charge accumulation in the CH•••HC bay region. This is consistent with (i) the analysis of the CH--HC contacts in the Zn^{II} and Ni^{II} complexes with nitrilotri-3-propanoic acid;[36,37,109] where the charge outflow from the occupied σ(C–H) orbital to the adjacent empty σ^*(C–H) was noted with, on average, $\Delta E_{orb} = -1.35$ kcal mol^{-1},[109] (ii) the picture from the VB-based approach by Echeverría *et al* for alkanes,[34] as well as with (iii) dominating exchange term from IQA analysis.

Because the combined ETS-NOCV method allows a partitioning of the total orbital interaction term from ETS, ΔE_{orb}^{T}, in a basis set of NOCV, we decided to look for trends between the partitioned ΔE_{orb}^{k} (the energy of a specific NOCV channel) and interatomic distances. Because there are four Zn–O bonds in ZnL with corresponding ΔE_{orb}^{k} values of –11.78, –10.88, –11.78 and –10.88 kcal mol^{-1}, the average value of –11.3 (indicated as ΔE_{orb}^{k*}) was used in further analysis. For the chelating Zn–N bonds, two separate and similar in nature NOCV contributions per coordinated ligand were always identified. The corresponding ΔE_{orb}^{k} values (e.g. –37.7 and – 14.3 kcal mol^{-1} in ZnL) were averaged to describe a single Zn–N bond formed by a ligand. In

the case of ZnL_2 and ZnL_3, two and three ΔE_{orb}^{k*} values, respectively, were obtained and they were averaged to obtain the energy contribution per a statistical Zn–N bond in a complex – see Table 6. Individual NOCV-based channels, their corresponding isovalues and associated ΔE_{orb}^{k} values are displayed in Table S10 of the SI.

We have established that, for both coordination bonds, the stabilizing contribution made by the orbital interaction energy, ΔE_{orb}^{k*}, decreases when going from ZnL to ZnL_3. As an example, for a single Zn–N bond, ΔE_{orb}^{k*} increased by +7.3 kcal·mol^{-1} from –26.0 kcal·mol^{-1} in ZnL to an average value of –18.7 kcal·mol^{-1} in ZnL_3. (Significantly weaker Zn–O coordination bonds follow the same trend).

Table 6. Orbital interaction energies for all Zn–L coordination bonds in Zn^{II} complexes with 2,2′-bipyridyl (L)

Complex	Atoms	Fragmentation Scheme	$\Delta\rho_k$ channel	ΔE_{orb}^{k*} [a]
ZnL	Zn–(N5,N6)	*(2)-bpy*	1,2	–26.0
	Zn–O1	*(2)-OH$_2$*	1	–11.78
	Zn–O2	*(2)-OH$_2$*	1	–10.88
	Zn–O3	*(2)-OH$_2$*	1	–11.78
	Zn–O4	*(2)-OH$_2$*	1	–10.88
			Average	*–11.3*
ZnL$_2$	Zn–(N1,N2)	*(2)-bpy*	1,2	–22.42
	Zn–(N3,N4)	*(2)-bpy*	1,2	–22.50
			Average	*–22.46*
	Zn–O5	*(2)-OH$_2$*	1	–8.62
	Zn–O6	*(2)-OH$_2$*	1	–8.53
			Average	*–8.57*
ZnL$_3$	Zn–(N55,N56)	*(2)-bpy*	1,2	–18.71
	Zn–(N57,N58)	*(2)-bpy*	1,2	–18.71
	Zn–(N59,N60)	*(2)-bpy*	1,2	–18.69
			Average	*–18.7*

The orbital interaction energy term, ΔE_{orb} from the ETS-NOCV theory, describes the energy changes associated with inter-fragment occupied and virtual orbital mixing as well as intra-fragment density rearrangement. Therefore, when combined with the visual deformation densities shown in Figure 8, they can be interpreted as a stabilizing interaction involving occupied orbitals on the ligands (bipyridyl and H_2O) and the unoccupied virtual orbitals on Zn^{II}. As our data shows, this stabilization is inversely proportional to the length of the coordination bonds (see Figure S14 in the SI) and this corresponds well with trends in the relevant values for ρ_{BCP} (from QTAIM), E_{int}^{AB} (from IQA) and ρ_{ICP}^{AB} (from NCI).

Table 7. Averaged orbital interaction energies for CH•••O and CH•••HC intramolecular interactions in Zn^{II} complexes with 2,2′-bipyridyl (L)

Complex	Atoms	Fragmentation Scheme	$\Delta\rho_k$ channel	ΔE_{orb}^{k*} [a]
ZnL	H8–O1, H24–O3	*(2)-bpy (N5,N6)*	12	−0.9
			14,16	−0.6
			Sum	*−1.5*
	H14–H18	*(7)-pyr*	21,23	−4.3
ZnL$_2$	H42–O5	*(2)-bpy (N1,N2)*	15	−1.1
			17,18	−0.6
			Sum	*−1.7*
	H24–O6	*(2)-bpy (N3,N4)*	15	−1.1
			17,18	−0.6
			Sum	*−1.7*
	H16–H18, H36–H32	*(7)-pyr*	23,25,26,27	−5.5

ZnL₃	H8–H12, H26–H30, H44–H48	*(7)-pyr*	26,27,28,29,30	−7.4

ZnL$_3$	H8–H12, H26–H30, H44–H48	*(7)-pyr*	26,27,28,29,30	−7.4

[a] *In kcal·mol^{-1}*

    Representative set of data obtained for relevant NOCV channels for the CH•••O and CH•••HC intramolecular interactions is collected in Table 7. It is important to stress that the CH•••O and CH•••HC interactions (i) are characterized by a set of distinctive NOCV channels and (ii) might not shows deformation density changes on every occurrence of a specific interaction in the molecule. For instance, the NOCV channels $\Delta\rho_{26}$ and $\Delta\rho_{27}$ (shown in Figure S15 of the SI) describe the energy associated with deformation densities only for two CH•••HC interactions, even though three CH--HC contacts are present in ZnL$_3$. Consequently, to generate $\Delta E_{\text{orb}}^{k*}$ describing the orbital energy contribution per a single interaction, the ($\Delta E_{\text{orb}}^{26}$ + $\Delta E_{\text{orb}}^{27}$) value was divided by two. The full procedure used to generate $\Delta E_{\text{orb}}^{k*}$ for CH•••O and CH•••HC interactions is illustrated in Tables S11 and S12 of the SI.

    $\Delta E_{\text{orb}}^{k*}$ for CH•••O becomes more negative by 0.2 kcal·mol^{-1}, from −1.5 kcal·mol^{-1} in ZnL to −1.7 kcal·mol^{-1} in ZnL$_2$, as the d(CH--O) becomes shorter. Importantly, trends observed in $\Delta E_{\text{orb}}^{k*}$ obtained for intramolecular interactions (when going from ZnL to ZnL$_3$) follow those generated by the QTAIM, IQA and NCI analyses when ρ_{BCP}, $E_{\text{int}}^{\text{H,O}}$ and $\rho_{\text{ICP}}^{\text{H,O}}$ were used, respectively.

    The stabilizing orbital energies obtained per a single CH•••HC interaction are about three times larger when compared with the $\Delta E_{\text{orb}}^{k*}$ values obtained per a single CH•••O interaction. This correlates very well with the IQA data showing predominant stabilizing contribution coming from the $V_{\text{XC}}^{\text{H,H}}$ term and an excellent $\Delta E_{\text{orb}}^{k*}$(CH•••HC) vs. d(CH--HC) relationship was obtained – see Figure S16 in the SI).

Hancock and Nikolayenko[28] reported recently that there is no evidence of the CH•••HC interaction in *cis*-BPy (the NBO method by Weinhold[110] was used). This is not entirely surprising because NBO considers only two atomic blocks of a density matrix (the remaining elements vanish);[111] clearly, NBO is not suitable for that purpose. On the other hand, the NOCV scheme[70,71] (which is partially similar to NBO[112]) revealed the charge accumulation in the CH--HC interatomic bonding region because this method is based on a full density matrix expressed in the fragment orbital basis set; hence, it shows an important role of off-diagonal density matrix elements in a description of weak diatomic interactions. It is important to point out that Weinhold demonstrated recently that indeed, when using NBO combined with QTAIM (so called NBCP method), one can obtain consistent picture showing some local electronic stabilization stemming from a CH•••HC interaction.[113]

Recent work by Danovich *et al*[34] demonstrated that '*the classical dispersion mechanism does not explain the head-on bonding homo-nuclear H--H interactions between alkanes larger than methane*'. These contacts in alkanes were characterized by the total bonding energy of up to ~3 kcal mol^{-1} and this can be used in support of our interpretation of the CH•••HC interactions in metal complexes. To this effect, let us finally analyze leading NOCV deformation densities for the dimer of dodecahedrane, one of the examples considered in Ref. 34. Figure S17 (in the SI) clearly shows formation of three, although weak ($\Delta E_{orb}(1)$ = -0.7 kcal mol^{-1} and $\Delta E_{orb}(2)$ = -0.25 kcal mol^{-1}) CH•••HC interactions, qualitatively analogous to those obtained for ZnL, ZnL$_2$ and ZnL$_3$ complexes (see Figure 11a). Note that Danovich *et al*,[35] using a VB method, also showed electron charge reorganization between interacting C–H bonds of larger alkanes clusters as a major contribution to the interaction. Interestingly, these results demonstrate qualitatively very

much the same changes in electron density due to formation of CH--HC contacts in different molecular systems.

It is important to point out that our ETS-NOCV results do not contradict the important knowledge emphasizing the significance of Pauli repulsion within CH--HC contacts as found in biphenyl. Here we have identified non-negligible electronic stabilization due to CH•••HC interactions in Zn-complexes; similar NOCV channels were found by us for planar biphenyl (Figure S18 in the SI). Such an observation was not noted before by Bickelhaupt and others[42–46] when using a 'pure' ETS/EDA scheme; thus, ETS/EDA scheme combined with NOCV seems to provide more detailed information on the electronic reorganization due to CH--HC contacts.

Finally, let us briefly discuss ETS-NOCV based results originating from four-fragment resolution, i.e. in each case (ZnL, ZnL$_2$, ZnL$_3$) an interaction between four units will be considered [ZnL - interaction between Zn^{2+}/bpy/(H$_2$O)$_2$/(H$_2$O)$_2$; ZnL$_2$ - Zn^{2+}/bpy/bpy/(H$_2$O)$_2$; ZnL$_3$ - Zn^{2+}/bpy/bpy/bpy]. Such an approach enables us to comparatively estimate role of electrostatic stabilization as well as π-electron delocalization in the stabilization of these complexes. It is clear from Table S13 in the SI that electrostatic stabilization increases most rapidly, by 40.9 kcal mol^{-1} (from ZnL to ZnL$_3$); similar is valid for π-stabilization [$\Delta E_{\mathrm{orb}}(\pi)$], however, the effect is less pronounced, by 30.9 kcal mol^{-1} (visualized for ZnL in Figure S19 of the SI). Accordingly, the total interaction energy becomes more negative when going from ZnL to ZnL$_3$. The variation in $\Delta E_{\mathrm{total}}$ (it is an interaction energy between the distorted fragments) correlates very well with an increase in the values of the experimental data;[1] the enthalpy of complex formation becomes more negative and overall formation constants increase from ZnL to ZnL$_3$ – see Figure S20 in the SI.

3.6. Spin-Spin ^{1}J(C–H) coupling constants. Due to the fact that the nature of homopolar CH--HC close contacts is so controversial, we have decided to provide an alternative view of density reorganization from the ^{1}H NMR spectroscopic perspective. Namely, we have calculated based on ADF program[72–74] one-bond ^{1}J(C–H) coupling constants for C–H connections involved in the CH--HC bridge. It has been proven experimentally and computationally that ^{1}J(C–H) spin-spin coupling constants are suitable to detect weak interactions, such as agostic C–H•••M (M = metal), hydrogen bonds (C–H•••D, D = electron donor) or hyperconjugation effects [σ(C–H)→ σ*(C–H)].[84–87] In these contacts an existence of the interaction is manifested by decrease in ^{1}J(C–H) coupling constants due to the interaction of C–H bond with adjacent moiety (metal, lone pair, or, like in our case, another C–H bond). Such interactions result in weakening of C–H bonds (either due to charge depletion from occupied σ(C–H) orbital or due to population of the empty σ*(C–H)).[84–87] It can clearly be seen from Table S14 of the SI that ^{1}J(C–H) coupling constant (at X3LYP/TZ2P) decreases from 177.06 Hz (for ZnL) to 173.87 Hz (for ZnL$_3$) (similar trend is valid for BP86/TZ2P), what further supports our observation on the increase in charge depletion from clashing σ(C–H) bonds when going from ZnL to ZnL$_3$. Similar trend, but less pronounced, is true when considering dimer of dodecahedron; namely, ^{1}J(C–H) values for C–H bonds involved in the close CH--HC contact are smaller (by ~1.5 Hz) than for the non-clashing C–H units (Figure S21 in the SI). It should be noted that when considering agostic interactions of the type CH•••M one can obtain far more significant lowering in ^{1}J(C–H) values due to interaction with metal, even by 30-40 Hz;[85] however, it is not surprising as this type of interactions is much stronger (~15–20 kcal mol^{-1})[85,86] as compared to the subtle stabilization arising from CH--HC contacts (~2–3 kcal mol^{-1}). Furthermore, the change of ^{1}J(C–H) values by

3–4 Hz is certainly not negligible as it falls in the regime of hyperconjugation (what can lead to the Perlin effect).[84]

4. Conclusions

The physical nature of coordination, covalent and intramolecular interactions in the ZnL_n complexes with 2,2′-bipyridyl were investigated based on the real space, topological methods (QTAIM, IQA and NCI) and ETS-NOCV charge and energy decomposition scheme. We found consistently from above approaches that:

- Both, coordination bonds, Zn–O, Zn–N, as well as CH•••O and CH•••N interactions were found to be of a stabilizing nature, in each case diatomic interaction energies $E_{int}^{AB} < 0$. Stabilizing contribution of these diatomic intramolecular interactions toward the overall electronic energy of complexes increases from ZnL to ZnL_3, but an opposite trend is observed for both coordination bonds (as found from QTAIM, IQA, NCI, and ETS-NOCV).

- The relative strength of bonding interactions (Zn–N and Zn–O) was recovered fully by all techniques; Zn–N is stronger than Zn–O, followed by much weaker intramolecular interactions.

- Predominant ionic character of the coordination bonds and intramolecular CH•••O, CH•••N interactions was confirmed by IQA, QTAIM and ETS-NOCV.

- ETS-NOCV provided a textbook description of a classical covalent (C2—C2') and the coordination bonds.

- ETS-NOCV-picture of a physical nature of the CH•••O interaction (i) agrees with the Popelier's QTAIM-based description of a hydrogen bond[102] and (ii) also shows some covalent component, importance of which was also stressed by Grabowski.[108]

- Formation of CH--HC contacts leads to local electronic stabilization (that increases from ZnL to ZnL_3), as it was found from the ETS-NOCV, IQA and spin-spin $^1J(C–H)$ coupling constants.

Such interaction appeared to be unique among all intramolecular interactions (but the NCI picture does not correspond with that observed for typical van der Waals interactions); combined results from all four techniques clearly point at the local CH•••HC electronic stabilization as being by far the weakest among all considered here. The IQA method showed that $V_{XC}^{H,H}$ dominates and (in absolute value) is larger than $V_{cl}^{H,H}$ which was found slightly repulsive at the MP2 level (our IQA values describing CH--HC contacts correlate well with the experimental stability constants - see Figure S22 in the SI).

 - NOCV channels showed that formation of the CH--HC contacts is accompanied by significant polarization of C–H bonds (mixing of σ/σ*(C–H)), what leads to charge accumulation in the CH•••HC bay region; this is consistent with very recent report based on valence bond studies for larger alkanes[35] as well as with QTAIM data – Figure S23 in the SI.

 - Neither the region between 3,3′-hydrogen atoms nor the ligand appear to be strained but instead the NCI plots pointed at the coordination sphere where steric strain is most likely located.

 -Highly repulsive interaction between N-atoms of bpy was fully recovered by IQA and NCI (no QTAIM-defined AIL is observed).

We would like to emphasize that in our current study all techniques that we used provided predominantly detailed information on the major coordination (Zn–O, Zn–N) and intramolecular hydrogen bonding contributions (CH•••O and CH•••N) that control stability of Zn^{II}-complexes. However, when describing chemical bonds and interactions one must adopt some models[113,114] (methods containing approximations and very often inherent arbitrariness), hence the picture on the CH•••HC interactions must be further explored in both experimental and theoretical laboratories in order to definitely uncover the nature of homopolar XH•••HX interactions in different molecular systems. Nonetheless, due to an excellent agreement on multi-technique

description of physical nature and relative strength of all these interactions, one should be able now to embark on relevant investigations with an attempt to understand why e.g. 1,10-phenanthroline forms slightly more stable complexes (no H-clashes present) when compared with bpy.

Finally, we introduced here the exchange-interaction ratio, EIR, defined as $V_{XC}^{AB} / E_{int}^{AB}$, which can be used to identify an interatomic interaction as overall either locally (i) stabilizing when EIR > 0 (e.g. positive values of EIR are observed here for all intramolecular interactions), or (ii) destabilizing, as we observe here for the N-atom of bpy for which EIR < 0. We found that variation in the EIR values (when EIR > 0) appears to correlate with a classical interpretation of a strong covalent, ionic, or intermediate bonding interaction; the smaller EIR the larger degree of iconic character is observed, whereas a value well above 1 (when $|V_{XC}^{AB}| >> |E_{int}^{AB}|$) points at a predominantly or fully classical covalent bond (e.g. EIR is almost 2 for the C–C bond). Using the ETS-NOCV data, we proposed here a simple protocol which generates an averaged (or normalized) ΔE_{orb}^{k*} values describing the orbital energy contribution per a single interaction; we found that the ΔE_{orb}^{k*} values correlate very well with interatomic distances, hence also with QTAIM-defined topological properties at BCPs.

Supporting Information. The following additional information is available in the electronic Supporting Information: Brief theoretical background on QTIAM, IQA, NCI and ETS-NOCV, selected structural data for all ZnL_n complexes, ball-and-stick representations and additional molecular graphs for ZnL_n complexes, additional topological data for coordination bonds and intramolecular interactions, additional relationships between bond lengths, topological data and orbital deformation energies, IQA data for all relevant interactions and bonds, NCI isosurfaces and plots of the reduced density gradient, selected NOCV and NOCV orbital deformation

energies, ETS-NOCV description of ZnL_n complexes in four-fragment resolution, and calculated $^1J(C–H)$ coupling constants for the CH•••HC interactions in ZnL_n complexes and in dodecahedron at various levels of theory. This material is available free of charge via the Internet at http://pubs.acs.org.

Corresponding Authors

* E-mail: ignacy.cukrowski@up.ac.za (IC); mitoraj@chemia.uj.edu.pl (MM)

Author Contributions

The manuscript was written through equal contributions of all authors. All authors have given approval to the final version of the manuscript.

References

(1)   NIST Standard Reference Database 46. NIST Critically Selected Stability Constants of Metal Complexes Database; Version 8.0; R. M. Smith, A. E. Martell, Eds.; US Department of Commerce, National Institute of Standards and Technology: Gaithersburg, MD, 2004.

(2)   Meyer, T. J. Chemical Approaches to Artificial Photosynthesis. *Acc. Chem. Res.* **1989**, *22*, 163–170.

(3)   Wrighton, M. S. J. Photoelectrochemistry: Inorganic Photochemistry at Semiconductor Electrodes. *Chem. Ed.* **1983**, *60*, 877–881.

(4)   Long, N. J. Organometallic Compounds for Nonlinear Optics—The Search for En-lightenment! *Angew. Chemie Int. Ed. Engl.* **1995**, *1*, 21–38.

(5)   Howard, S. T. Conformers, Energetics, and Basicity of 2, 2'-Bipyridine. *J. Am. Chem. Soc.* **1996**, *118*, 10269–10274

(6)   Kalenik, J.; Pawełka, Z. Solvent Influence on the Conformational Equilibrium of 2, 2′-Bipyridine. *J. Mol. Liq.* **2005**, *121*, 63–68

(7)   Labat, F.; Lainé, P. P.; Ciofini, I.; Adamo, C. Spectral Properties of Bipyridyl Ligands by Time-Dependent Density Functional Theory. *Chem. Phys. Lett.* **2006**, *417*, 445–451

(8)   C. Blanchet-Boiteux, P. Friant-Michel, A. Marsura, J-B. Regnouf-de-Vains, M. F. Ruiz-López. Theoretical Study of Solvent Effects on the Conformational Equilibrium and Electronic Spectra of 2, 2′-Bipyridine Derivatives. *J. Mol. Struct.* (THEOCHEM) **2007**, *811*, 169–174.

(9)   Galasso, V.; De Alti, G.; Bigotto, A. MO Calculations on the Preferred Conformation and Electronic Structure of Phenylpyridines and Bipyridines. *Tetrahedron* **1971**, *27*, 991–997.

(10)   Jaime, C.; Font, J. Empirical Force Field Calculations (MM2-V4) on Biphenyl and 2, 2′-Bipyridine. *J. Mol. Struct.* **1989**, *195*, 103–110.

(11)   Benedix, R.; Birner, P.; Birnstock, F.; Hennig, H.; Hofmann, H. J. Quantum Chemical Calculations for the Determination of the Molecular Structure of Conjugated Compounds:

Part XIV. On the Conformational Structure of α-Diimine Ligands. *J. Mol. Struct*. **1979**, *51*, 99–105.

(12) Benedix, R.; Birner, P.; Hennig, H. Quantum Chemical Investigations of the Conformational Structure of Protonated 2, 2'-Bipyridine. *J. Mol. Struct.* **1982**, *90*, 65–69.

(13) Barone, V.; Lelj, F.; Commisso, L.; Russo, N.; Caulletti, C.; Piancastelli, M. N. Experimental and Theoretical Approach to the Electronic Structure and the Molecular Conformation of Azabiphenyls. Assymetric Bipyridines. *Chem. Phys.* **1985**, *96*, 435–445.

(14) Zahn, S.; Reckien, W.; Kirchner, B.; Staats, H.; Matthey, J.; Lützen, A. Towards Allosteric Receptors: Adjustment of the Rotation Barrier of 2, 2′-Bipyridine Derivatives. *Chem. Eur. J.* **2009**, *15*, 2572–2580.

(15) Alkorta, I.; Elguero, J.; Roussel, C. A Theoretical Study of the Conformation, Basicity and NMR Properties of 2, 2′-, 3, 3′- and 4, 4′-Bipyridines and Their Conjugated Acids. *Comput. Theoret. Chem.* **2011**, *966*, 334–339.

(16) Göller, A. H.; Grummt, U. W. Torsional Barriers in Biphenyl, 2, 2′-Bipyridine and 2-Phenylpyridine. *Chem. Phys. Lett.* **2000**, *321*, 399–405.

(17) Göller, A.H.; Grummt, U. W. Detailed Energy Decomposition of the Rotational Barrier in 2, 2′-Bipyridine: A Density Functional Study. *Chem. Phys. Lett.* **2002**, *354*, 233–242.

(18) Chung, G.; Lee, D. Molecular Structures of 2,2-Bipyridine and its Anion Radical: Multiconfiguration-SCF Calculations. *Bull. Korean Chem. Soc.* **2008**, *29*, 2419–2422.

(19) Irving, H.; Mellor, D. H. The Stability of Metal Complexes of 1, 10-Phenanthroline and its Analogues. Part I. 1, 10-Phenanthroline and 2, 2′-Bipyridyl. *J. Chem. Soc*. **1962**, 5222–5237.

(20) Palmer, R. A.; Piper, T. S. 2, 2'-Bipyridine Complexes. I. Polarized Crystal Spectra of Tris (2, 2'-bipyridine) copper (II),-nickel (II),-cobalt (II),-iron (II), and-ruthenium (II). *Inorg. Chem.* **1966**, *5*, 864–878.

(21) Sone, K.; Utsuno, S.; Ogura, T. Absorption Spectra of Some Mixed Chelates of Copper (II). *J. Inorg. Nucl. Chem.* **1969**, *31*, 117–126.

(22) Griesser, R.; Sigel, H. Ternary Complexes in Solution. VIII. Complex Formation Between the Copper (II)-2, 2'-Bipyridyl 1: 1 Complex and Ligands Containing Oxygen and/or Nitrogen Donor Atoms. *Inorg. Chem.* **1970**, *9*, 1238–1243.

(23) Martin, R. B.; Prados, R. Some Factors Influencing Mixed Complex Formation. *J. Inorg. Nucl. Chem*. **1974**, *36*, 1665–1670.

(24) Hancock, R. D.; Martell, A. E. Ligand Design for Selective Complexation of Metal Ions in Aqueous Solution. *Chem. Rev.* **1989**, *89*, 1875–1914.

(25) Buist, D.; Williams, N. J.; Reibenspies, J. H.; Hancock, R. D. Control of Metal Ion Size-Based Selectivity Through Chelate Ring Geometry. Metal Ion Complexing Properties of 2, 2′-Biimidazole. *Inorg. Chem.* **2010**, *49*, 5033–5039.

(26) Cockrell, G. M.; Zhang, G.; VanDerveer, D. G.; Thummel, R. P.; Hancock, R. D. Enhanced Metal Ion Selectivity of 2, 9-Di-(Pyrid-2-Yl)-1, 10-Phenanthroline and its Use as a Fluorescent Sensor for Cadmium (II). *J. Am. Chem. Soc*. **2008**, *130*, 1420–1430.

(27) Del Piero, S.; Di Bernardo, P.; Fedele, R.; Melchior, A.; Polese, P.; Tolazzi, M. Affinity of Polypyridines Towards Cd^{II} and Co^{II} Ions: A Thermodynamic and DFT Study. *Eur. J. Inorg. Chem.* **2006**, 3738–3745.

(28) Hancock, R. D.; Nikolayenko, I. V. Do Nonbonded H--H Interactions in Phenanthrene Stabilize It Relative to Anthracene? A Possible Resolution to this Question and Its Implications for Ligands such as 2, 2′-Bipyridyl. *J. Phys. Chem. A* **2012**, *116*, 8572−8583.

(29) Zhurova, E. A.; Matta, C. F.; Wu, N.; Zhurov, V. V.; Pinkerton, A. A. Experimental and Theoretical Electron Density Study of Estrone. *J. Am. Chem. Soc.* **2006**, *128*, 8849–8861.

(30) Matta, C. F.; Hernández-Trujillo, J.; Tang, T. H.; Bader, R. F. W. Hydrogen–Hydrogen Bonding: A Stabilizing Interaction in Molecules and Crystals. *Chem. Eur. J.* **2003**, *9*, 1940–1951.

(31) Bader, R. F. W. Bond Paths are Not Chemical Bonds. *J. Phys. Chem. A* **2009**, *113*, 10391–10396.

(32) Pendás, A. M.; Francisco, E.; Blanco, M. A.; Gatti, C. Bond Paths as Privileged Exchange Channels. *Chem. Eur. J.* **2007**, *13*, 9362–9371.

(33) Cortés-Guzmán, F.; Hernández-Trujillo, J.; Cuevas, G. The Nonexistence of Repulsive 1, 3-Diaxial Interactions in Monosubstituted Cyclohexanes. *J. Phys. Chem. A* **2003**, *107*, 9253–9256.

(34) Echeverría, J.; Aullón, G.; Danovich, D.; Shaik, S.; Alvarez, S. Dihydrogen Contacts in Alkanes are Subtle but Not Faint. *Nat. Chem.* **2011,** *3*, 323–330.

(35) Danovich, D.; Shaik, S.; Neese, F.; Echeverría, J.; Aullón, G.; Alvarez, S. Understanding the Nature of the CH⋯HC Interactions in Alkanes. *J. Chem. Theory Comput.* **2013**, *9*, 1977–1991.

(36) Cukrowski, I.; Govender, K. K. A Density Functional Theory-and Atoms in Molecules-Based Study of NiNTA and NiNTPA Complexes Toward Physical Properties Controlling Their Stability. A New Method of Computing a Formation Constant. *Inorg. Chem.* **2010**, *49*, 6931–6941.

(37) Cukrowski, I.; Matta, C. F. Hydrogen–Hydrogen Bonding: A Stabilizing Interaction in Strained Chelating Rings of Metal Complexes in Aqueous Phase. *Chem. Phys Lett.* **2010**, *499*, 66–69.

(38) Robertson, K. N.; Knop, O.; Cameron, T. S. CH•••HC Interactions in Organoammonium Tetraphenylborates: Another Look at Dihydrogen Bonds. *Can. J. Chem.* **2003**, *81*, 727–743.

(39) Robertson, K. N. Intermolecular Interactions in a Series of Organoammonium Tetraphenyl-borates. Ph.D. Thesis, Dalhousie University, Halifax, Canada, 2001.

(40) Zhurova, E. A.; Tsirelson, V. G.; Zhurov, V. V.; Stash, A. I.; Pinkerton, A. A. Chemical Bonding in Pentaerythritol at Very Low Temperature or at High Pressure: An Experimental and Theoretical Study. *Acta Cryst. B* **2006**, *62*, 513–520.

(41) Bader, R. F. W. *Atoms in Molecules: A Quantum Theory*; Oxford University Press: Oxford, 1990.

(42) Poater, J.; Solà, M.; Bickelhaupt, F. M. Hydrogen–Hydrogen Bonding in Planar Biphenyl, Predicted by Atoms-In-Molecules Theory, Does Not Exist. *Chem. Eur. J.* **2006**, *12*, 2889–2895.

(43) Poater, J.; Solà, M.; Bickelhaupt, F. M. A Model of the Chemical Bond Must Be Rooted in Quantum Mechanics, Provide Insight, and Possess Predictive Power. *Chem. Eur. J.* **2006**, *12*, 2902–2905.

(44) Grimme, S.; Mück-Lichtenfeld, C.; Erker, G.; Kehr, G.; Wang, H.; Beckers, H.; Willner, H. When Do Interacting Atoms Form a Chemical Bond? Spectroscopic Measurements and Theoretical Analyses of Dideuteriophenanthrene. *Angew. Chem. Int. Ed.* **2009**, *48*, 2592–2595.

(45) Jia, J.; Wu, H.; Chen, Z.; Mo, Y. Elucidation of the Forces Governing the Stereochemistry of Biphenyl. *Eur. J. Org. Chem.,* **2013**, *3*, 611–616.

(46) Poater, J.; Visser, R.; Solà, M.; Bickelhaupt, F. M. Polycyclic Benzenoids: Why Kinked is More Stable than Straight. *J. Org. Chem.,* **2007**, *72*, 1134–1142.

(47) Bader, R. F. W. Pauli Repulsions Exist Only in the Eye of the Beholder. *Chem. Eur. J.* **2006**, *12*, 2896–2901.

(48) Hernández-Trujillo, J.; Matta, C. F. Hydrogen–Hydrogen Bonding in Biphenyl Revisited. *Struct. Chem.* **2007**, *18*, 849–857.

(49) Cambridge Crystallographic Data Centre, 12 Union Road, Cambridge CB2 1EZ, U.K.

(50) McKee, W. C.; Schleyer, P. V. R. Correlation Effects on the Relative Stabilities of Alkanes. *J. Am. Chem. Soc.* **2013**, *135*, 13008–13014.

(51) Wolstenholme, D. J.; Traboulsee, K. T.; Hua, Y.; Calhoun, L. A.; McGrady G. S. Thermal Desorption of Hydrogen from Ammonia Borane: Unexpected Role of Homopolar B–H•••H–B Interactions. *Chem. Comm.*, **2012**, *48*, 2597–2599.

(52) Wolstenholme, D. J.; Titah, J. T.; Che, F. N.; Traboulsee, K. T.; Flogeras, J.; McGrady G. S. Homopolar Dihydrogen Bonding in Alkali-Metal Amidoboranes and Its Implications for Hydrogen Storage. *J. Am. Chem. Soc.* **2011**, *133*, 16598–16604.

(53) Wolstenholme, D. J.; Flogeras, J.; Che, F. N.; Decken, A.; McGrady G. S. Homopolar Dihydrogen Bonding in Alkali Metal Amidoboranes: Crystal Engineering of Low-Dimensional Molecular Materials. *J. Am. Chem. Soc.* **2013**, *135,* 2439–2442.

(54) Pichon A. Hydrogen Bonding: Unconventional Connections. *Nature Chemistry* **2013**, *5*, 250–250.

(55) Richardson, T. B.; de Gala, S.; Crabtree, R. H. Unconventional Hydrogen Bonds: Intermolecular BH•••HN Interactions. *J. Am. Chem. Soc.* **1995**, *117*, 12875–12876.

(56) Jonas, J.; Frenking, G.; Reetz M. T. Comparative Theoretical Study of Lewis Acid-Base Complexes of BH_3, BF_3, BCl_3, $AlCl_3$, and SO_2. *J. Am. Chem. Soc.* **1994**, *116*, 8741–8753.

(57) Mitoraj M. P. Bonding in Ammonia Borane: An Analysis Based on the Natural Orbitals for Chemical Valence and the Extended Transition State Method (ETS-NOCV). *J. Phys. Chem. A* **2011**, *115*, 14708–14716.

(58) Morrison, A. M.; Siddick, C. A. Dihydrogen Bonds in Solid BH_3NH_3. *Angew. Chem. Int. Ed.* **2004**, *43*, 4780–4782.

(59) Merino, G.; Bakhmutov, V. I.; Vela, A. Do Cooperative Proton-hydride Interactions Explain the Gas-solid Structural Difference of BH_3NH_3? *J. Phys. Chem. A.* **2002**, *106*, 8491–8494.

(60) Popelier P. L. A. Characterization of a Dihydrogen Bond on the Basis of the Electron Density. *J. Phys. Chem. A*, **1998**, *102*, 1873–1878.

(61) Bühl, M.; Steinke, T.; Schleyer, P. V. R.; Boese, R. Solvation Effects on Geometry and Chemical Shifts. An Ab Initio/IGLO Reconciliation of Apparent Experimental Inconsistencies on H_3B•••NH_3. *Angew. Chem. Int. Ed.* **1991**, *30*, 1160–1161.

(62) Guerra, D.; David, J.; Restrepo, A. $(H_3N–BH_3)_4$: The Ammonia Borane Tetramer. *Phys. Chem. Chem. Phys.* **2012**, *14*, 14892–14897.

(63) Blanco, M. A.; Pendás, A. M.; Francisco, E. Interacting Quantum Atoms: A Correlated Energy Decomposition Scheme Based on the Quantum Theory of Atoms in Molecules. *J. Chem. Theory Comput.* **2005**, *1*, 1096–1109.

(64) Francisco, E.; Pendás, A. M.; Blanco, M. A. A Molecular Energy Decomposition Scheme for Atoms in Molecules. *J. Chem. Theory Comput.* **2006**, *2*, 90–102.

(65) Pendás, A. M.; Blanco, M. A.; Francisco, E. Chemical Fragments in Real Space: Definitions, Properties, and Energetic Decompositions. *J. Comput. Chem.* **2007**, *28*, 161–184.

(66) Johnson, E. R.; Keinan, S.; Mori-Sánchez, P.; Contreras-García, J.; Cohen, A. J.; Yang, W. Revealing Noncovalent Interactions. *J. Am. Chem. Soc.* **2010**, *132*, 6498–6506.

(67) Contreras-García, J.; Johnson, E. R.; Keinan, S.; Chaudret, R.; Piquemal, J. P.; Beratan, D.; Yang, W. NCIPLOT: A Program for Plotting Noncovalent Interaction Regions. *J. Chem. Theory Comput.* **2011**, *7*, 625–632.

(68) Gillet, N.; Chaudret, R.; Contreras-García, J.; Yang, W.; Silvi, B.; Piquemal, J. P. Coupling Quantum Interpretative Techniques: Another Look at Chemical Mechanisms in Organic Reactions. *J. Chem. Theory Comput.* **2012**, *8*, 3993−3997.

(69) Contreras-García, J.; Yang, W.; Johnson, E. R. Analysis of Hydrogen-Bond Interaction Potentials from the Electron Density: Integration of Noncovalent Interaction Regions. *J. Phys. Chem. A* **2011**, *115*, 12983–12990.

(70) Mitoraj, M.; Michalak, A. Natural Orbitals for Chemical Valence as Descriptors of Chemical Bonding in Transition Metal Complexes. *J. Mol. Model.* **2007**, *13,* 347–355.

(71) Mitoraj, M.; Michalak, A.; Ziegler, T. A Combined Charge and Energy Decomposition Scheme for Bond Analysis. *J. Chem. Theory Comput.* **2009**, *5*, 962–975.

(72) te Velde, G.; Bickelhaupt, F. M.; van Gisbergen, S. J. A.; Fonseca Guerra, C.; Baerends, E. J.; Snijders, J. G.; Ziegler, T. Chemistry with ADF. *J. Comp. Chem.* **2001**, *22*, 931–967.

(73) Fonseca Guerra, C.; Snijders, J.G.; te Velde, G.; Baerends, E. J. Towards an Order-N DFT Method. *Theoretical Chemistry Accounts* **1998**, *99*, 391–403.

(74) Baerends, E. J.; Ziegler, T.; Autschbach, J.; Bashford, D.; Bérces, A.; Bickelhaupt, F. M.; Bo, C.; Boerrigter, P. M.; Cavallo, L.; Chong, D. P.; Deng, L.; Dickson, R. M.; Ellis, D. E.; van Faassen, M.; Fan, L.; Fischer, T. H; Fonseca Guerra, C.; Ghysels, A.; Giammona, A.; van Gisbergen, S. J. A.; Götz, A. W.; Groeneveld, J. A.; Gritsenko, O. V.; Grüning, M.;

Gusarov, S.; Harris, F. E.; van den Hoek, P.; Jacob, C. R.; Jacobsen, H.; Jensen, L.; Kaminski, J. W.; van Kessel, G.; Kootstra, F.; Kovalenko, A.; Krykunov, M. V.; van Lenthe, E.; McCormack, D. A.; Michalak, A.; Mitoraj, M.; Neugebauer, J.; Nicu, V. P.; Noodleman, L.; Osinga, V. P.; Patchkovskii, S.; Philipsen, P. H. T.; Post, D.; Pye, C. C.; Ravenek, W.; Rodríguez, J. I.; Ros, P.; Schipper, P. R. T.; Schreckenbach, G.; Seldenthuis, J. S.; Seth, M.; Snijders, J. .; Solà, M.; Swart, M.; Swerhone, D.; te Velde, G.; Vernooijs, P.; Versluis, L.; Visscher, L.; Visser, O.; Wang, F.; Wesolowski, T. A.; van Wezenbeek, E. M.; Wiesenekker, G.; Wolff, S. K.; Woo, T. L.; Yakovlev, A. L. ADF2012, SCM, Theoretical Chemistry, Vrije Universiteit, Amsterdam, The Netherlands, http://www.scm.com

(75) Van Lenthe, E.; Baerends, E. J. Optimized Slater-Type Basis Sets for the Elements 1–118. *J. Comp. Chem.* **2003**, *24*, 1142–1156.

(76) Chong, D. P. Augmenting Basis Set for Time-Dependent Density Functional Theory Calculation of Excitation Energies: Slater-Type Orbitals for Hydrogen to Krypton. *Mol. Phys*. **2005**, *103*, 749-761.

(77) Xu, X.; Goddard, W. A., III. The X3LYP Extended Density Functional for Accurate Descriptions of Nonbond Interactions, Spin States, and Thermochemical Properties. *Proceedings of the National Academy of Sciences* **2004**, *101*, 2673–2677

(78) Xu, X.; Zhang, Q.; Muller, R. P.; Goddard, W. A., III. An Extended Hybrid Density Functional (X3LYP) with Improved Descriptions of Nonbond Interactions and Thermodynamic Properties of Molecular Systems. *J. Chem. Phys.* **2005**, *122*, 014105–014120.

(79) Plumley, J. A.; Dannenberg, J. J. A Comparison of the Behavior of Functional/Basis Set Combinations for Hydrogen-Bonding in the Water Dimer with Emphasis on Basis Set Superposition Error. *J. Comp. Chem.* **2011**, *32*, 1519–1527

(80) Grimme, S. Semiempirical GGA-Type Density Functional Constructed with a Long-Range Dispersion Correction. *J. Comp. Chem.* **2006**, *27*, 1787–1799.

(81) Gaussian 09, Revision A.1, Frisch, M. J.; Trucks, G. W.; Schlegel, H. B.; Scuseria, G. E.; Robb, M. A.; Cheeseman, J. R.; Scalmani, G.; Barone, V.; Mennucci, B.; Petersson, G. A.; Nakatsuji, H.; Caricato, M.; Li, X.; Hratchian, H. P.; Izmaylov, A. F.; Bloino, J.; Zheng, G.; Sonnenberg, J. L.; Hada, M.; Ehara, M.; Toyota, K.; Fukuda, R.; Hasegawa, J.; Ishida, M.; Nakajima, T.; Honda, Y.; Kitao, O.; Nakai, H.; Vreven, T.; Montgomery, J. A., Jr.; Peralta, J. E.; Ogliaro, F.; Bearpark, M.; Heyd, J. J.; Brothers, E.; Kudin, K. N.; Staroverov, V. N.; Kobayashi, R.; Normand, J.; Raghavachari, K.; Rendell, A.; Burant, J. C.; Iyengar, S. S.; Tomasi, J.; Cossi, M.; Rega, N.; Millam, J. M.; Klene, M.; Knox, J. E.; Cross, J. B.; Bakken, V.; Adamo, C.; Jaramillo, J.; Gomperts, R.; Stratmann, R. E.; Yazyev, O.; Austin, A. J.; Cammi, R.; Pomelli, C.; Ochterski, J. W.; Martin, R. L.; Morokuma, K.; Zakrzewski, V. G.; Voth, G. A.; Salvador, P.; Dannenberg, J. J.; Dapprich, S.; Daniels, A. D.; Farkas, Ö.; Foresman, J. B.; Ortiz, J. V.; Cioslowski, J.; Fox, D. J. Gaussian, Inc., Wallingford CT, 2009.

(82) AIMAll (Version 12.08.21), Keith, T. A. TK Gristmill Software, Overland Parks KS, USA, 2012 (aim.tkgristmill.com)

(83) Humphrey, W.; Dalke, A.; Schulten, K. VMD: Visual Molecular Dynamics. *J. Molec. Graphics*, **1996**, *14.1*, 33–38.

(84) Juaristi, E.; Cuevas, G. Manifestations of Stereoelectronic Interactions in ^{1}JC–H One-Bond Coupling Constants. *Acc. Chem. Res.* **2007**, *40*, 961–970.

(85) Clot, E.; Eisenstein, O. Agostic Interactions from a Computational Perspective: One Name, Many Interpretations. *Struct. Bond.* **2004**, *113,* 1–36.

(86) Mitoraj, M.; Michalak, A.; Ziegler, T. On the Nature of the Agostic Bond between Metal Centers and β-Hydrogen Atoms in Alkyl Complexes. An Analysis Based on the Extended Transition State Method and the Natural Orbitals for Chemical Valence Scheme (ETS-NOCV). *Organometallics* **2009**, *28*, 3727–3733.

(87) Scherer, W.; Herz, V.; Brück, A.; Hauf, C.; Reiner, F.; Altmannshofer, S.; Leusser, D.; Stalke, D. The Nature of β-Agostic Bonding in Late-Transition-Metal Alkyl Complexes. *Angew. Chem. Int. Ed.* **2011**, *50*, 2845–2849.

(88) Espinosa, E.; Alkorta, I.; Elguero, J.; Molins, E. From Weak to Strong Interactions: A Comprehensive Analysis of the Topological and Energetic Properties of the Electron Density Distribution Involving X–H··· F–Y Systems. *J. Chem. Phys.* **2002**, *117*, 5529–5542.

(89) Cremer, D.; Kraka, E. Chemical Bonds without Bonding Electron Density—Does the Difference Electron-Density Analysis Suffice for a Description of the Chemical Bond? *Angew. Chem. Int. Ed. Engl.* **1984**, *23*, 627–628.

(90) Cremer, D.; Kraka, E. A Description of the Chemical Bond in Terms of Local Properties of Electron Density and Energy. *Croat. Chem. Acta.* **1984**, *57*, 1259–1281.

(91) Bone, R. G. A.; Bader, R. F. W. Identifying and Analyzing Intermolecular Bonding Interactions in Van Der Waals Molecules. *J. Phys. Chem.* **1996**, *100*, 10892–10911.

(92) Bobrov, M. F.; Popova, G. V.; Tsirelson, V. G. A Topological Analysis of Electron Density and Chemical Bonding in Cyclophosphazenes $P_nN_nX_{2n}$ (X= H, F, Cl; N= 2, 3, 4). *Russ. J. Phys. Chem.* **2006**, *80*, 584–590.

(93) Macchi, P.; Sironi, A. Chemical Bonding in Transition Metal Carbonyl Clusters: Complementary Analysis of Theoretical and Experimental Electron Densities. *Coord. Chem. Rev.* **2003**, *238-239*, 383–412.

(94) Jenkins, S.; Morrison, I. The Chemical Character of the Intermolecular Bonds of Seven Phases of Ice as Revealed by Ab Initio Calculation of Electron Densities. *Chem. Phys. Lett.* **2000**, *317*, 97–102.

(95) Flaig, R.; Koritsanszky, T.; Dittrich, B.; Wagner, A.; Luger, P. Intra-and Intermolecular Topological Properties of Amino Acids: A Comparative Study of Experimental and Theoretical Results. *J. Am. Chem. Soc.* **2002**, *124*, 3407–3417.

(96) Espinosa, E.; Molins, E.; Lecomte, C. Hydrogen Bond Strengths Revealed by Topological Analyses of Experimentally Observed Electron Densities. *Chem. Phys. Lett.* **1998**, *285*, 170–173.

(97) Bader, R. F. W.; Essén, H. The Characterization of Atomic Interactions. *J. Chem. Phys.* **1984**, *80*, 1943–1960.

(98)   Kitaura, K.; Morokuma, K. A New Energy Decomposition Scheme for Molecular Interactions within the Hartree-Fock Approximation. *Int. J. Quantum Chem.* **1976**, *10*, 325–340.

(99)   Parr, R. G.; Ayers, P. W.; Nalewajski, R. F. What is an Atom in a Molecule? *J. Phys. Chem. A* **2005**, *109*, 3957–3959.

(100)   Matta, C. F.; Bader, R. F. W. An Experimentalist's Reply to "What is an Atom in a Molecule?". *J. Phys. Chem. A* **2006**, *110*, 6365–6371

(101)   Sherrill, C. D.; Takatani, T.; Hohenstein, E. G. An Assessment of Theoretical Methods for Nonbonded Interactions: Comparison to Complete Basis Set Limit Coupled-Cluster Potential Energy Curves for the Benzene Dimer, the Methane Dimer, Benzene− Methane, and Benzene− H_2S. *J. Phys. Chem. A.,* **2009**, *113*, 10146–10159.

(102)   Koch, U.; Popelier, P. L. A. Characterization of CHO Hydrogen Bonds on the Basis of the Charge Density. *J. Phys. Chem.* **1995**, *99*, 9747–9754.

(103)   Otero-de-la-Roza, A.; Johnson, E. R.; Contreras-García, J. Revealing Non-Covalent Interactions in Solids: NCI Plots Revisited. *Phys. Chem. Chem. Phys.* **2012**, *14*, 12165–12172.

(104)   Fukui, K. The Path of Chemical Reactions - the IRC Approach. *Acc. Chem. Res.* **1981**, *14*, 363–368.

(105)   Grabowski, S. J. Properties of a Ring Critical Pointas Measures of Intramolecular H-Bond Strength. *Monatshefte für Chemie,* **2002**, *113*, 1373–1380.

(106)   Palusiak, M.; Krygowski, T. M. Application of AIM Parameters at Ring Critical Points for Estimation of π-Electron Delocalization in Six-Membered Aromatic and Quasi-Aromatic Rings. *Chem.–Eur. J.,* **2007**, *13*, 7996–8006.

(107)   Howard, S. T.; Krygowski, T. M. Benzenoid Hydrocarbon Aromaticity in terms of Charge Density Descriptors. *Can. J. Chem.,* **1997**, *75*, 1174–1181.

(108)   Grabowski, S. J. What is the Covalency of Hydrogen Bonding? *Chem. Rev.* **2011**, *111*, 2597–2625.

(109)   Cukrowski, I.; Govender, K. K.; Mitoraj, M. P.; Srebro, M. QTAIM and ETS-NOCV Analyses of Intramolecular CH···HC Interactions in Metal Complexes. *J. Phys. Chem. A* **2011**, *115*, 12746–12757.

(110)   Foster, J. P.; Weinhold, F. Natural Hybrid Orbitals. *J. Am. Chem. Soc.* **1980**, *102*, 7211–7218.

(111)   Weinhold, F. Natural Bond Critical Point Analysis: Quantitative Relationships between Natural Bond Orbital-based and QTAIM-based Topological Descriptors of Chemical Bonding. *J. of Comp. Chem.* **2012**, *33*, 2440–2449.

(112)   Glendening, E. D.; Landis, C. R.; Weinhold, F. Natural Bond Orbital Methods. *Wiley Interdisciplinary Reviews: Computational Molecular Science* **2012**, *2,* 1–42.

(113)   Frenking, G.; Krapp, A. Unicorns in the World of Chemical Bonding Models. *J. Comp. Chem.* **2007**, *28*, 15–24.

(114)   Frenking, G.; Fröhlich, N. The Nature of the Bonding in Transition-Metal Compounds. *Chem. Rev.* **2000**, *100*, 717–774.